First Principle Modelling of Materials and Processes in Dye-Sensitized Photoanodes for Solar Energy and Solar Fuels

Mariachiara Pastore

Université de Lorraine & CNRS, SRSMC, TMS, Boulevard des Aiguillettes, 54506 Vandoeuvre-lès-Nancy, France; mariachiara.pastore@univ-lorraine.fr; Tel.: +33-3-83-68-43-77

Abstract: In the context of solar energy exploitation, dye-sensitized solar cells and dye-sensitized photoelectrosynthetic cells offer the promise of low-cost sunlight conversion and storage, respectively. In this perspective we discuss the main successes and limitations of modern computational methodologies, ranging from hybrid and long-range corrected density functionals, GW approaches and multi-reference perturbation theories, in describing the electronic and optical properties of isolated components and complex interfaces relevant to these devices. While computational modelling has had a crucial role in the development of the dye-sensitized solar cells technology, the theoretical characterization of the interface structure and interfacial processes in water splitting devices is still at its infancy, especially concerning the electron and hole transfer phenomena. Quantitative analysis of interfacial charge separation and recombination reactions in multiple metal-oxide/dye/catalyst heterointerfaces, thus, undoubtedly represents the compelling challenge in the field of modern computational material science.

1. Introduction

Answering the request of globally-increasing energy consumption, while reducing the environmental impact, undoubtedly represents one of the most compelling societal and technological challenges [1–3]. Since 2002, the world energy consumption rate of 13.5 terawatts (TW) is predicted to increase to at least two-fold by 2050, due to the growth of the world population and economic developments [4]. On a global scale, about 85% of the energy source comes from fossil fuels, but their costs and the serious concerns in terms of impact on environment and human health, as well as the directly-related geo-political problems, call for a progressive increase in renewable energy exploitation. As a matter of fact, all of the renewable energy areas are extending, with an estimated renewable share of final energy consumption of about 19% (modern technologies and traditional biomass being at 10% and 9%, respectively) [2]. Among renewable energy sources, the sun is our ultimate resource: sunlight strikes the Earth's surface at a continuous rate of 1.2×10^5 TW, largely exceeding our current worldwide power demand; it is inexhaustible and rather well distributed over the planet. To be exploitable, however, solar energy needs to be converted to heat, electricity, or chemical bonds (fuels) [5–7], and while its conversion to heat is straightforward, an effective production of electricity and fuels from sunlight poses severe issues. The first problem is related to the maximum efficiency that can be achieved converting sunlight into electricity and fuels: considering the average solar spectral distribution, the most favourable absorption region is about 885 nm (1.4 eV) which, in principle, would allow for a 33% energy conversion efficiency [8]. Moreover, to achieve large-scale industrialization and commercialization, the materials employed in solar devices should also be cheap and abundant

in the Earth's crust with a reduced environmental impact and possibly high long-term stability. In the context of solar energy exploitation, dye-sensitized solar cells (DSCs) [9,10] and dye-sensitized photoelectrosynthetic cells (DSPECs) [5,11,12] offer the promise of low-cost sunlight conversion and storage, respectively. Since the seminal paper by O'Regan and Grätzel in 1991 [9], hybrid/organic photovoltaic devices have attracted significant research interest, which has recently lead to the launch of the first commercial product. The basic functioning mechanism of a DSC is depicted in Figure 1 along with a representation of the different competing forward (solid black lines) and back (dotted red lines) electron transfer (ET) processes. The heart of the cell is represented by the photoanode, which consists of a mesoporous oxide layer (7–10 μm), usually composed of TiO_2 or ZnO nanoparticles deposited onto a transparent conducting oxide on a glass or plastic substrate. The nanocrystalline oxide is sensitized by a monolayer of dyes (D), chemically bound to the semiconductor nanoparticles. Upon solar light absorption, the adsorbed sensitizers are able to inject the photo-excited electrons in the manifold of the conduction band (CB) states of the semiconductor, typically at the femtosecond time scale. Injected electrons travel through the mesoporous film and are collected by the conductive layer of the photoanode electrode, while the oxidized dye (D^+) is rapidly reduced by the electron mediator donor in solution [13] or by the hole transporting material (HTM) in solid-state devices. The collected electrons flow in the external circuit, producing a photocurrent, and reach the counter-electrode, where the circuit is closed by the reduction of the electron mediator acceptor [14,15].
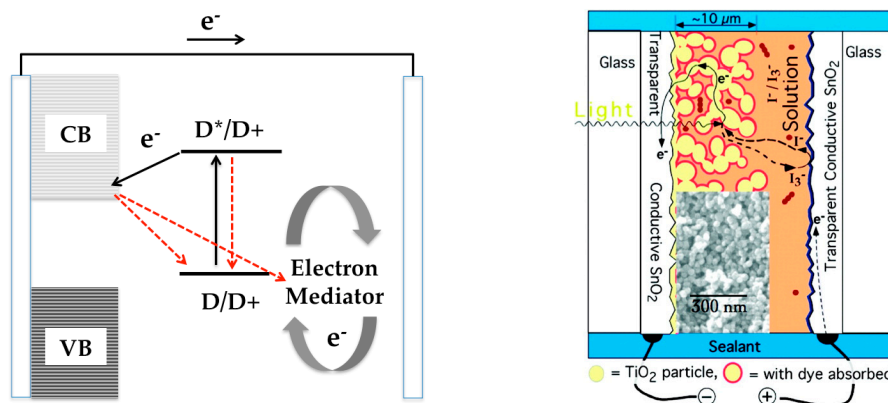

Figure 1. (**left**) Illustrative diagram of the functioning mechanism of a typical n-type DSC. The different competing forward (solid black lines) and back (dotted red lines) electron transfer reactions are also indicated; (**right**) Physical composition of a DSC and SEM image of the dye-sensitized TiO_2 film (adapted from [15]).

The same idea of exploiting a molecular (or supramolecular) system (light absorber) grafted on solid electrodes (n- and p-type semiconductors for the photoanode and photochatode, respectively) in contact with an electrolytic solution can be also implemented in a photo-electrochemical cell (PEC) to produce H_2: such a configuration is schematically depicted in Figure 2. In this type of PEC, a dye adsorbed on the surface of a wide band-gap semiconductor (typically TiO_2) absorbs the solar radiation to produce an electron and a hole, which are injected into the semiconductor and catalyst, respectively: oxygen is produced at the dye-sensitized semiconductor photoanode, while hydrogen is produced, by a catalyst at the cathode, where photogenerated electrons are collected.

The reactions taking place at the electrodes of a DSPEC are reported in the following, where h^+ and e^- are, respectively, the photo-generated holes and electrons.

$$2H_2O + 4h^+ \rightarrow O_2 + 4H^+ \qquad E^0 = 1.23 \text{ V vs. NHE}$$

$$4H^+ + 4e^- \rightarrow 2H_2 \qquad E^0 = 0 \text{ V vs. NHE}$$

The presence of multiple solid/liquid active interfaces makes DSCs and DSPECs inherently complex systems, where the individual characteristics of catalysts, photosensitizers, and semiconductors,

as well as the interfacial properties of the assembled photoelectrodes strongly interplay in determining the overall device efficiencies [16]. General guidelines to optimally design and combine the interface "players" (i.e., dyes [17–21]), metal oxides [22,23], electrolytes [24,25], and catalysts [26–29]) are derived from simple considerations on the material's structural, redox, and optical properties [30–33]. In addition to the optimization of standalone components, however, optimizing the energy level matching, the morphology, and the optical properties of the functionalized interface is crucial to boost the device efficiency [34–42].
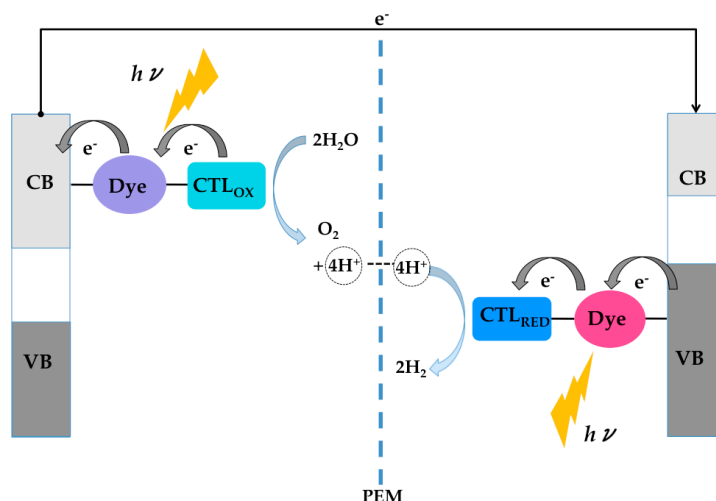

Figure 2. Scheme of a DSPEC for H_2 production composed by a photoanode and a phtocathode decorated with dye-CTL assemblies. PEM is a proton exchange membrane.

From a computational point of view, modern first principles computational methodologies, essentially relying on density functional theory (DFT) and its time dependent extension (TDDFT), are able to describe most of the target characteristics of the individual systems (dyes, catalysts, semiconductors, etc.) [16,43–59] and of their active interfaces [16,41,43,47,60–79]. The information extracted from these calculations serve as the basis for the explicit simulation of the photo-induced electron transfer by means of quantum or non-adiabatic dynamics. Different combinations of electronic structure/excited states and nuclear dynamics descriptions have been applied to molecule-functionalized metal oxide interfaces [69,72,80–84]. In most cases these approaches rely either on semi-empirical Hamiltonians [69,85] or on the time-dependent propagation of single particle DFT orbitals [86,87], with the nuclear dynamics being described within mixed quantum-classical [69,80,85,86] or fully-quantum mechanical approaches [87]. Real-time propagation of the TDDFT excited states [88] has also emerged as a powerful tool to study photoinduced electron transfer events, with applications to dye-sensitized interfaces based on mixed quantum-classical dynamics [82,89].

In the last years, increased computing power along with efficient implementations of highly-correlated post Hartree-Fock [90–93] and post DFT methodologies [94,95], has opened the way to accurate benchmark studies on the isolated components [59,96–98], as well as on the hybrid interfaces [74,99,100] relevant to dye-sensitized devices. While, however, computational modelling has played a prominent role in the development of the DSC technology, the understanding of the interfacial processes in DSPEC is still at its infancy, especially for what concerns the electron and hole transfer phenomena, which are central to efficient device functioning. Most of the published computational modeling works so far are, indeed, focused on the characterization of the water oxidation/proton reduction reaction mechanisms, [57,101–104] with only a few studies reporting the interaction between the catalysts, dyes, and semiconductors [67,68,71,72].

In this perspective, we shell review recent activity in the computational modelling of dyes and dye-sensitized interfaces in DSCs and DSPECs, discussing at the same time the successes and the still unsolved issues faced by modern quantum chemistry methodologies.

2. Dye's Optical Properties

2.1. Organic Dyes

Efficient sensitizers for DSCs have to be endowed with a strong absorption in the UV-VIS region of the solar spectrum associated to long-lived, charge-separated, excited states with the correct directionality (toward the metal-oxide surface). These requirements are, usually, fulfilled by using a D-π-A structure (hereafter termed push-pull), where the donor group (D) is an electron-rich unit, the electron-acceptor group (A) is covalently bound to the semiconductor surface and they are linked through a conjugated bridge (π). Accurate prediction of excitation energies of push-pull dyes is challenging for both TDDFT [43,44,96,105] and wave-function approaches due to the strong charge transfer nature of the electronic transitions and associated orbital relaxation effects [106,107].

The inclusion of a fix percentage (from ≈20% to ≈50%) of non-local Hartree-Fock exchange (HFexc) in the functional [108] and the use of range-separated hybrid functionals [109–113] are the most commonly employed strategies to practically overcome these drawbacks. Within the latter family, the so called 'optimally tuned' functionals, put forward by Baer, Kronik, and co-workers [114], are grounded on a different idea: the range separation parameter is determined in a non-empirical way, by minimizing the difference between the highest occupied molecular orbital (HOMO) energy (ε_{HOMO}) and the vertical ionization potential (IP). Optimally-tuned RS approaches have been successfully applied to different problematic test cases [54,62,115–118], where standard functionals are known to dramatically fail. Considering, for instance, the two prototypical push-pull dyes, D102 and JK2, featuring different donor and acceptor units (Figure 3a), the comparison between the calculated and experimental excitation energies in Table 1 clearly show that the choice of, and the identification of, the "best" functional is not straightforward.
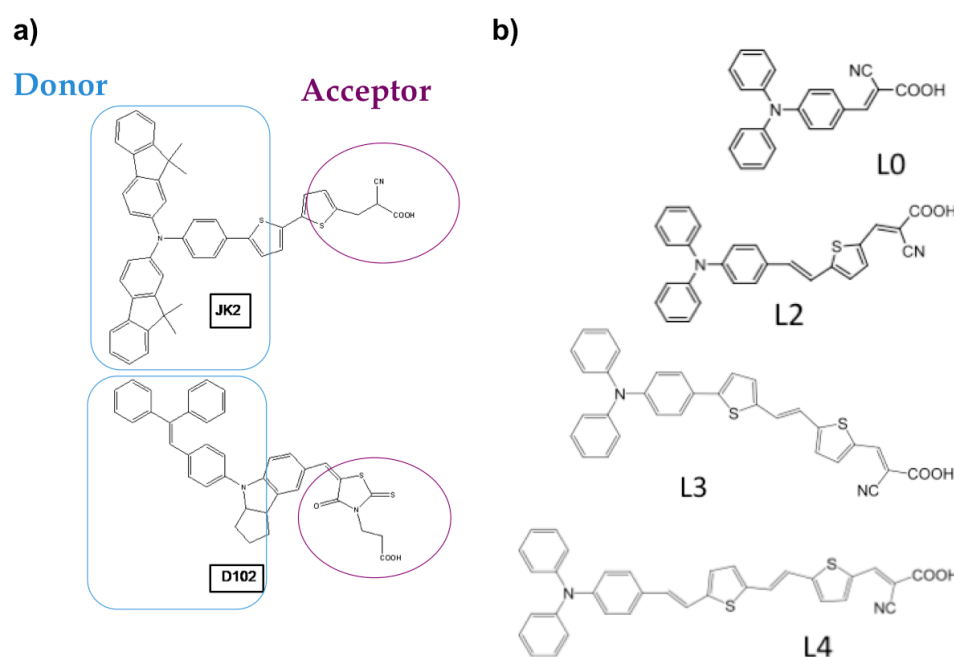

Figure 3. Molecular structure of JK2 and D102 (**a**); and of L0, L2, L3, and L4 (**b**).

Table 1. TDDFT excitation energies (in eV) of the lowest excited state of JK2 and D102 in gas phase and EtOH solution for the protonated (1H) and deprotonated (0H) form compared to the experimental absorption maxima. Data from [43].

Dye	B3LYP			MPW1K			CAM-B3LYP			Exp. (EtOH)
	1H		0H	1H		0H	1H		0H	
	Vac	Solv	Solv	Vac	Solv	Solv	Vac	Solv	Solv	
JK2	1.99	1.82	2.26	2.60	2.45	2.81	2.78	2.62	2.94	2.84 [119]
D102	2.61	2.29	2.37	3.07	2.78	2.89	3.11	2.86	2.90	2.53 [120]

These data demonstrate that different systems might require different functionals to be properly treated and, thus, TDDFT fails in a priori prediction of the optical properties of push-pull organic molecules. A careful method validation is, thus, mandatory, including solvent effects and a careful analysis of the anchoring group acid-base chemistry. In fact, while bulk solvent effects (polar and non-polar environments) are usually quantitatively captured by implicit models [121], a realistic modeling of explicit solute-solvent interactions (i.e., specific hydrogen bonding) might be required in protic solvents [41,96,122–125].

Similar difficulties are also encountered in the calculation of the oxidation potentials [44] whose accuracy has been demonstrated to deteriorate as the conjugation length of the molecule increases, even when long-range corrected, or hybrid functionals with a higher percentage of non-local exchange, are employed. Many-body perturbation theory (MBPT), within the GW approximation [94], although more computationally demanding, represents a solid framework to improve the DFT description of the quasi-particle (QP) energy levels. GW [126,127] was used to calculate the ionization potential and electron affinity (Table 2) of a series of triphenyl-based push-pull dyes with increasing degree of electronic conjugation (L0, L2, L3, and L4 in Figure 3b). QP energy levels were computed at the so-called G_0W_0 level [95] on top of DFT ground-state calculations, performed with the BLYP functional. All of the DFT calculations discussed in the following were performed using the pw.x code of the Quantum ESPRESSO software package [128] (see [74] for further details). As a matter of fact, a dependence of the G_0W_0 results on the chosen starting exchange and correlation functional has been widely reported [129–132]. In particular, hybrid exchange and correlation functionals appear as the most promising in giving consistent G_0W_0 results. In the following calculations, however, we have chosen as starting point a local exchange and correlation functional to keep a coherent description with the calculations of the molecules adsorbed on the TiO_2 surface (see [74]), for which calculations with hybrid functionals could not be afforded.

Table 2. Vertical ionization potentials (IP) and electron affinities (EA) calculated with the GW method for the L0, L2, L3, and L4 dyes.

Dye	IP (eV)	EA (eV)
L0	6.87	1.66
L2	6.48	2.31
L3	6.37	2.28
L4	6.21	2.21

Electron photoemission measurements [133] on related TPA-based dyes bearing the rhodanine-3-acetic acid acceptor group give an IP of 6.75 eV for the dye corresponding to L0 and an IP of 6.50 eV for the dye corresponding to L2. As shown from the calculated IPs in Table 2, an increase in the length of the linker moiety corresponds to a decrease of the calculated IP, thus providing a trend comparable to the experimental oxidation potentials, even though the measured quantities are in solution and also account for the change in energy due to structural relaxations.

2.2. Transition Metal Complexes

Ru(II)-polypyridyl complexes have been primarily employed as dye sensitizers [52,122,134–137]. The unsurpassed performance of the [Ru(4,4′-COOH-2,2′-bpy)$_2$(NCS)$_2$] complex, the N3 dye [134] (Figure 4), played a central role in significantly advancing the DSCs field, with solar to electric power efficiencies exceeding 11% [52,137].
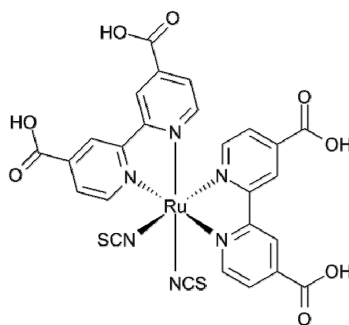
Figure 4. Molecular structure of the N3 dye.

From the computational point of view, the electronic, optical, and redox properties of N3, as well as analogous ruthenium polypyridyl dyes, have been successfully characterized at the DFT/TDDFT level of theory, employing functionals with a moderate fraction of HF exchange (e.g., B3LYP [138], PBE0 [139], M06 [140]) and resorting to implicit solvation models [51,52,122,141–146]. The need of including the surroundings in the calculations has been widely highlighted [142,144,147–152]: solvent usually induces a sizeable shift (even larger than 1 eV) to higher energies of the otherwise underestimated MLCT excitations, thus delivering calculated spectra in overall better agreement with the experimental ones. It seems, however, that a similarly strong solvation effect does not apply to metal-centred (MC) or inter-ligand (IL) transitions, which also behave differently with the increase of the HF percentage in the functional [151]. On the other hand, the large size of the systems and the presence of a large number of almost degenerate excited states of different nature [153] have clearly limited the number of correlated wavefunction-based benchmark calculations in the gas phase reported so far [97,151,154–157]. Recently, exploiting the efficient implementation of the second order n-electron valence state perturbation theory (NEVPT2) method [90–92], in the ORCA program package [93], we have reported state-of-the-art highly-correlated excited states calculations on the low-lying transitions of the N3 dye both in vacuo and water solution, with the aim of shedding light onto the solvation effects on the optical properties of N3. The detailed computational strategy can be found in [59], here we only remark that, for the results reviewed here, the zero order wavefunctions were defined by state average (SA)-CASSCF calculations including the ground and the lowest 14 excited states (hereafter termed CAS_15). The 7 highest-occupied and the 5 lowest-unoccupied molecular orbitals were included into the active space, resulting in a space of 14 active electrons into 12 active orbitals. The effect of the solvent was investigated by comparing CAS_15/NEVPT2 and B3LYP excited state calculations within the Tamm-Dancoff approximation implemented in ORCA for hybrid functionals. As discussed in [51] and shown by the calculated TDA-B3LYP spectra in the top panel of Figure 5, inclusion of solvent strongly modifies the energies and nature of the frontier molecular orbitals (MO) at this level of theory, reshaping and blue-shifting the calculated absorption spectrum, which in solution nicely reproduces the experimental one. At the B3LYP level in vacuo, the three highest occupied almost degenerate molecular orbitals are basically localized on the NCS ligands with ca. 7% of Ru t_{2g} contribution, HOMO-3 is a pure NCS orbital and the inner set of quasi-degenerate HOMO-4, HOMO-5, and HOMO-6 have a mixed NCS-Ru nature with a significant metal-d contribution, namely 58%, 67%, and 65%, respectively. The lowest-energy unoccupied molecular orbitals are π* orbitals localized on the bipyridine ligands with sizable contribution from the carboxylic groups. Inclusion of the solvent strongly stabilizes (by about 0.7 eV) the HOMO, HOMO-1, and HOMO-2 and markedly modifies their character: the contribution from the ruthenium d orbitals increases from about 7% to about 35%. The HOMO-3 is still an almost pure NCS orbital and is stabilized by 0.9 eV passing from gas phase to water. The character and energy of the three almost degenerate HOMO-4, HOMO-5, and HOMO-6 basically is unchanged when the solvent effects are considered. Finally, the lowest unoccupied molecular orbitals (LUMOs) retain their bipyridine π* nature but are destabilized by about 0.3–0.4 eV. The calculated HOMO-LUMO energy gap thus increases by about 1 eV going from 1.36 eV

in gas phase to 2.32 eV in water. According to this electronic rearrangement in solution, the two lowest energy bands are originated by excited states with a mixed ligand-metal-to-ligand character, involving a neat CT from mixed NCS-Ru orbitals to the π* orbitals localized on the bypyridines. This results in a reduction of the dipole moment of the excited states compared to that of the ground states and, thus, in a blue shift in the excitation energies going from gas phase to polar solvents [51]. The notably improved agreement between the TDA spectrum in water and the experimental one is, however, not simply due to this expected hypsochromic shift, as is apparent in Figure 5 (left panel). Indeed, the change in the composition and energy of the ground state MOs gives rise to a marked rearrangement of the energy and intensity of the states underlying the two lowest-energy bands. The low content of Ru-d character in the three highest occupied Kohn–Sham molecular orbitals in gas phase, which is clearly the cause of the unreliable TDA spectrum (red line in Figure 5) seems to be, in fact, mainly related to orbital relaxation effects, which are instead, already taken into account at CASSCF level in gas phase, where the HOMO, HOMO-1, and HOMO-2 are essentially Ru t_{2g} orbitals [59].
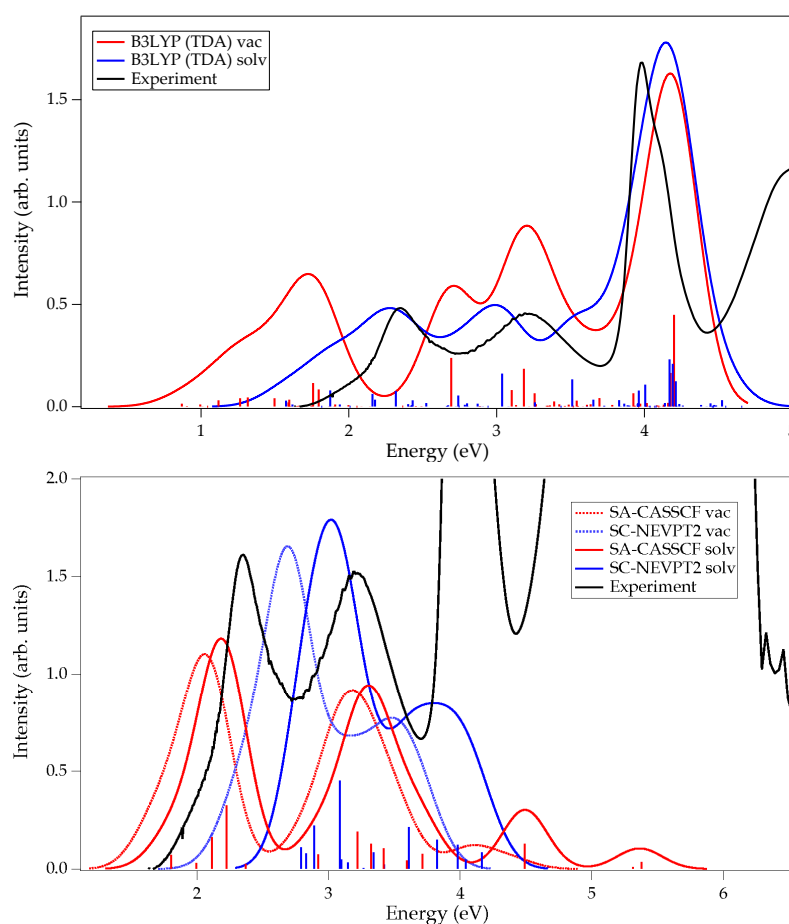

Figure 5. (**top**) Calculated TDA-B3LYP optical absorption spectra in gas phase (red line) and water solution (blue line) of the N3 complex compared with the experimental in water (black line), properly scaled to match the intensity of the first band of the spectrum in solution (blue line); (**bottom**) SA-CASSCF (red) and SC-NEVPT2 (blue) optical absorption spectra in gas phase (dotted lines) and water solution (full lines) of the N3 complex calculated by averaging over 15 states. Comparison with the experimental absorption spectrum is also reported. The spectra were simulated by a Gaussian broadening with σ = 0.17 eV. Vertical sticks correspond to the calculated excitation energies and oscillator strengths. Figure adapted from [59].

To further clarify this picture, and possibly disentangle the solvatochromism from the orbital polarization effects, we investigated the role of the solvent on the CASSCF wavefunction and NEVPT2

excitation energies. The calculated excitation energies and oscillator strengths compared to those obtained in gas phase, are plotted in the bottom panel of Figure 5, while band maxima and band separation are listed in Table 3, along with the B3LYP-TDA ones. We found that the overall picture obtained in gas phase still holds in water solution. At SA-CASSCF level, three intense states (excitations from the set of three HOMOs, having ca. 80% of Ru t_{2g} contribution, to the two lowest LUMOs, localized on the bipyridines) at 1.80, 2.11, and 2.23 eV are considerably blue-shifted (ca. 0.8–0.9 eV) by the pertubation correction at 2.79, 2.89, and 3.08 eV. At higher energies (between ca. 2.9 and 3.4 eV) four rather intense transitions appear, which still have pure metal to ligand charge transfer nature with excitations from the three lowest HOMOs to the higher-energy LUMO+4 and LUMO+5. These states, which give rise to the second band in the spectrum (bottom panel in Figure 5), also undergo a destabilization (by about 0.5 eV) at NEVPT2 level, where they are calculated at 3.34, 3.61, 3.82, and 3.92 eV, respectively. Then, state number 12, being sizably stabilized when the perturbation correction is applied going from 4.49 eV (CASSCF) to 2.83 eV (NEVPT2), has a strong multiconfiguration character. Finally, two weakly absorbing states (13 and 14) appear at 5.31/3.26 and 5.38/3.42 eV at the CASSCF/NEVPT2 level, respectively. As discussed for the gas phase results, these states, which are dramatically down-shifted by the perturbation, have a mixed ligand-metal-to-ligand nature, since they are mainly described by excitations from occupied orbitals having a dominant NCS contribution to bypiridine-localized virtual orbitals. The cause of their sizably overstabilization upon the perturbation correction has to be identified in core polarization effects. The present CASSCF/NEVPT2 results, even though with the limitation of a state-averaged optimization of the wavefunction (and, hence, of the solvent response) over states with rather different charge distributions, predict the expected blue-shift of the absorption spectrum going from gas phase to water solution, due to the over stabilization of the ground state in polar solvents. The effect of the solvent, however, does not substantially change the picture delivered by the gas phase calculations: the composition in terms of Ru-d and NCS contribution of the frontier occupied orbitals remains the same, as well as the nature of the excited states giving rise to the two low-energy bands. In other words, the NEVPT2 results in gas phase already provide a reliable description and assignation of the electronic structure and low-lying excited states of N3, whereas these are achieved in a DFT/TDDFT approach only by means of the solvent, which properly polarizes the ground state frontier MOs.

Table 3. Calculated and experimental (H_2O, pH = 1) absorption maxima (E_{max}) of the three UV-VIS absorption bands (I, II, and III) and the corresponding band separation (ΔE) for N3. All energies are in eV. Data are from [59].

		E_{max} (I)	E_{max} (II)	E (III)	ΔE (I-II)	ΔE (II-III)
Experimental (H_2O, pH = 1)		2.35	3.19	3.99	0.84	0.80
		15 states				
Calculated	SA-CASSCF solv	2.18	3.30	-	1.12	-
	SC-NEVPT2 solv	3.24	4.13	-	0.89	-
		TDA-B3LYP				
	Gas phase	1.72	2.70–3.20	4.17	-	-
	Water	2.27 [a]/2.39 [b]	2.99 [a]/2.95 [b]	4.14 [a]/3.98 [b]	0.72 [a]/0.56 [b]	1.15 [a]/1.03 [b]

[a] def2-SVP basis set; [b] def2-TZVP basis set.

Summarizing, at the CASSCF/NEVPT2 level, inclusion of the solvation effects leaves essentially unchanged the ground state electronic structure as well as the excited states picture found in vacuo, solely yielding the expected spectral shift to higher energies. In the light of these findings, the reason of the unreliable TDDFT spectrum calculated in vacuo is traced back to an inadequate ground state molecular orbital polarization, possibly coming from static correlation effects captured at the CASSCF level of theory, which can be achieved in the TDDFT framework only by inclusion of the solvent contribution. It is also worthwhile to stress here that our work also demonstrated that the main reason of the appreciable blue shift of the NEVPT2 absorption spectra is the SA-CASSCF definition of the zero

order wavefunctions, which, as a matter of fact, represents the main limitation in the application of MRPT2 approaches to this kind of systems. In fact, to keep a satisfactory accuracy at perturbative level, a limited number of states (15–20) has to be included in the average procedure. More importantly, the states with a nature different to that of the majority of the states considered in the state-averaged optimization, for instance, the ground state, are badly described and are then liable to be overcorrected by the second-order perturbation.

3. Dye/TiO$_2$ Interfaces in DSCs

The interaction between the dye and the TiO$_2$ nanoparticles results into hybridization of their molecular orbitals with the consequent change in their relative energy level alignment. To account for this effect, the combined dye/TiO$_2$ system has to be treated as a whole. The first crucial step in this regard is the determination of the most favored adsorption geometry, which has a key role in the electronic coupling between the dye and the semiconductor and, thus, in the overall electron injection [61,158,159]. Additionally, the collective orientation of adsorbed dyes on the semiconductor surface strictly depends on the anchoring motif, possibly affecting the rate and effectiveness of parasitic recombination reactions [160–162]. Finally, the sensitizer's grafting group should establish a stable binding of the dye onto the metal oxide surface, thus ensuring long-term stability of the cell [163–165]. Investigation of the adsorption of organic dyes onto TiO$_2$ cluster models [161,162,166], has largely shown that the bidentate bridging adsorption mechanism with proton transfer to a nearby surface oxygen is the energetically favored one (Figure 6), while the monodentate anchoring is usually predicted to be less stable, although some dependency on the employed methodology can be outlined [166], For Ru(II) sensitizers different adsorption modes onto the TiO$_2$ surface can be found: while homoleptic dyes, such as N3 or N719, can adsorb on TiO$_2$ using carboxylic anchoring groups residing on different bipyridine ligands and hence using up to three carboxylic groups (Figure 6c) [159,167], heteroleptic dyes, e.g., N621, C106, or Z907, necessarily adsorb via carboxylic groups residing on the same bipyridine (two carboxylic groups, Figure 6d) [168,169].
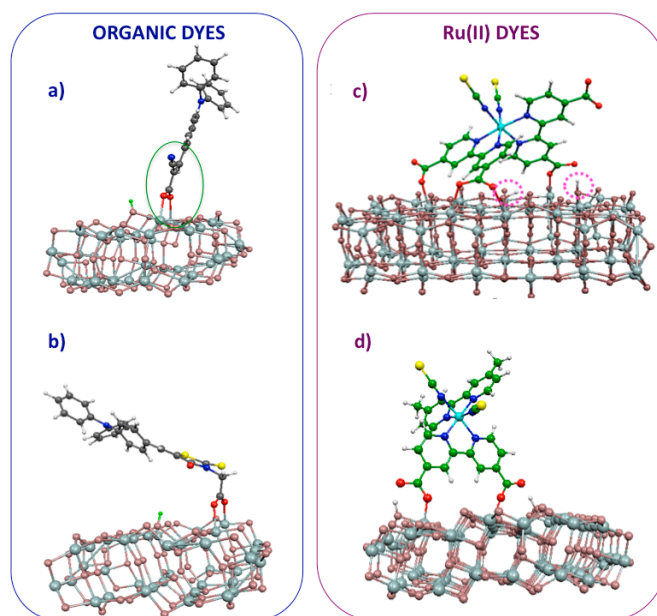

Figure 6. (**left**) Adsorption geometries of two differently-anchored organic dyes: a cyanoacrylic (**a**) and a 3-acetic rhodanine (**b**) acids anchored dyes; (**right**) adsorption of two prototypical Ru(II)-complexes with three points anchoring (**c**) and two monodentate points anchoring (**d**).

From an electronic structure point of view, when a dye is anchored to a semiconductor surface, two effects might interplay: (i) the electrostatic (EL) effect, due to the dye dipole moment; and (ii) the effect

of the CT between the dye and the semiconductor, which may accompany the dye/semiconductor bond formation. It has been shown [170] that in the dye-TiO$_2$ interaction, ground state CT effects induce a conduction band shift which for the bidentate anchored systems is much larger than the one calculated for the monodentate ones: this, as well as the electrostatic effect, contributes to their larger upward conduction band shift (ca. 0.2 eV compared to 0.02 eV, respectively). It, thus, turns out that the CT component of the CB shift may, in fact, be the dominant one (60%–70% of the total), with a relative variability comparable to that exhibited by the electrostatic component.

Moreover, a part from the position of the TiO$_2$ CB, having an accurate estimation of the relative energy levels alignment is crucial when the efficiency of the dye's excited state electron injection has to be evaluated. The position of the dye's LUMO with respect to the CB states determines, in fact, both the probability (dictated by the number of acceptor semiconductor states) and the electronic coupling for the electron transfer rate (see Equation (1) below). Here we report the calculation of the level alignment for a prototypical organic dye (L0) adsorbed onto the TiO$_2$ surface. As illustrated above, the GW method correctly describes the all-organic dyes in the gas-phase, and the accurate band gap of bulk anatase TiO$_2$ has also been calculated (in the range 3.6–3.7 eV) [171–173]. The measured [174] experimental optical band gap (3.25 eV) is, however, a somewhat smaller value than the GW gap that does not contain the electron-hole interaction [58]. The calculated electronic band gap for the slab in the dye/TiO$_2$ system is 4.9 eV, which is 0.6 eV larger than that calculated for the bare slab. Such an increase is due to hybridization effects, which are important when the size of the slab is comparable to that of the dye. In Figure 7 (right panel), we report the positions with respect to the vacuum level of the energy levels of the HOMO and LUMO of the dye and of the valence band maximum (VBM) and conduction band minimum (CBM) of the TiO$_2$ slab, as calculated with DFT-BLYP and with the GW method. We report these values in the cases of the isolated dye, of the sole slab, and of the adsorbed dye/slab system. The relative order of the levels is the same, except for the CBM of the sole slab and the L0 HOMO of the isolated molecule, which turns out to be almost degenerate within DFT-BLYP. For the case of the adsorbed L0 dye, the relative position of the L0 HOMO with respect to the VBM and CBM of the TiO$_2$ is quite different: closer to the VBM in the GW case and closer to the CBM in the DFT-BLYP case. When the L0 dye is adsorbed on the slab, the energy levels of the VBM of the TiO$_2$ remains almost unchanged while the level of the molecular HOMO (which is almost unchanged from the HOMO of the isolated molecule) is slightly pushed towards higher energies of 0.4 eV. As the HOMO is localized on the L0 dye such effect should be ascribed to the interaction with the image charge [175]. In this case, we register a similar shift of 0.4 eV towards lower energies. Hence, the HOMO-LUMO molecular gap is smaller by 0.8 eV after adsorption. In addition to the energy level alignment, it is also interesting to examine how GW and BLYP describe the hybridization between the adsorbate and substrate states, which is another key factor determining the rate of electron injection. In fact, according to the Newns and Anderson model [176,177], assuming that a single dye state (LUMO) couples with the semiconductor CB, one can get an estimate of the injection rate by simply analysing the broadening of the PDOS relative to the LUMO of the sensitizer [74]. The calculated PDOS broadening, $\hbar\Gamma$ (described by a Lorentzian distribution), gives an effective measure of the strength of the electronic coupling between the sensitizer and the TiO$_2$ substrate and can be directly translated into electron-transfer time [176,177] by using the relation:

$$\tau(\text{fs}) = 658/\Gamma(meV)$$

Figure 7b (left panel) displays the PDOSs calculated at the GW and BLYP levels and the corresponding Lorentzian distributions of the L0 LUMO. Apart from the ~1 eV shift of the energy levels discussed previously, GW and BLYP give a similar extent of LUMO broadening, GW predicting, however, a slightly more coupled system. The calculated Lorentzian broadening values are 0.246 eV and 0.231 eV for GW and BLYP, respectively, with corresponding estimated injection times of 2.67 fs and 2.85 fs, respectively, in agreement with the previously-reported ultrafast injection rates [49,178].
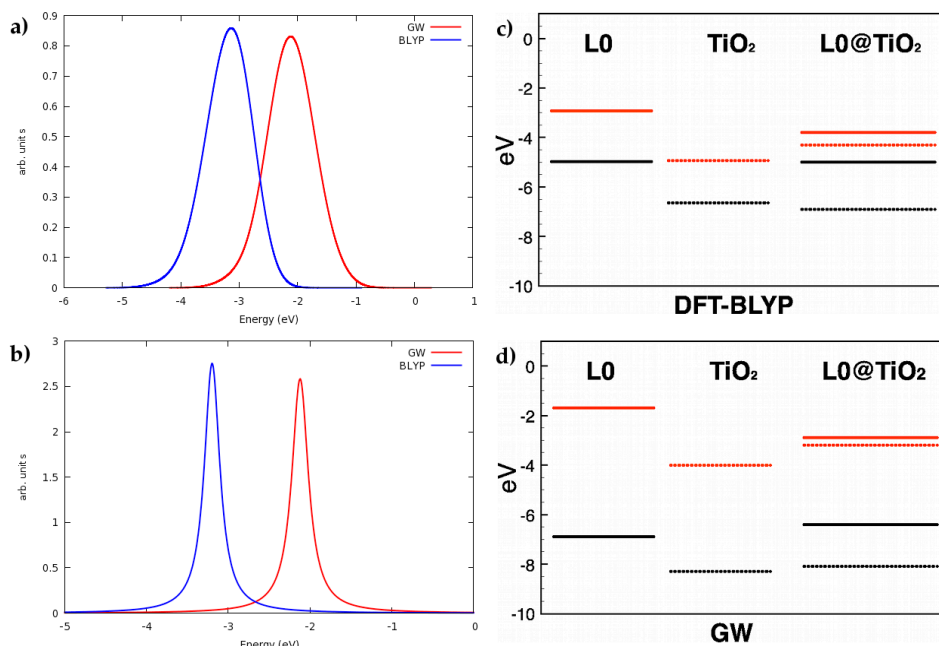
Figure 7. (**left**) L0@TiO$_2$ PDOS (**a**) and corresponding Lorentzian distribution (**b**) of the dye's LUMO. A Gaussian broadening of 0.3 eV has been used for the PDOS simulation (see text); (**right**) Position with respect to vacuum of the energy levels of the HOMO (bold-black) and LUMO (bold-red) of the L0 dye, and the VBM (dotted-black) and CBM (dotted-red) of the TiO$_2$ slab, reported for the isolated L0 dye, the sole slab, and the L0 dye adsorbed on the anatase TiO$_2$ (101) surface. (**c**) calculated with DFT-BLYP and (**d**) with the GW method. Adapted from [74].

Concerning the simulation of excited state properties, standard TDDFT approaches (B3LYP and PBE0) can accurately describe the optical properties and the system energy level alignment of Ru(II)-complexes grafted on the TiO$_2$ surfaces [43,68,179]. On the other hand, available TDDFT methods are not capable of delivering, at the same time, a balanced description of the dye/TiO$_2$ excited states and of the alignment of the dye excited states with the semiconductor manifold of unoccupied states [43]. While the standard B3LYP provides the correct alignment of the dye/semiconductor energy levels, along with a wrong dye's excitation energy, stronger hybrids or long-range corrected hybrids deliver the accurate prediction of the optical properties, but an unphysical picture of the interfacial energetics. These results are the consequence of a different and unbalanced description of the dye and semiconductor excited (or unoccupied) states, whereby highly conjugated dyes require a substantial amount of dynamic correlation to correct the inadequacy of the Kohn-Sham orbitals and deliver the correct excited state energy, while for TiO$_2$ the Kohn–Sham orbitals already represent an adequate description of the system's excited states.

4. TiO$_2$/Dye/Catalyst Multiple Interfaces in DSPECs

TiO$_2$-dye-catalyst interactions turn out to be crucial in a photoanode for water oxidation, where grafting of the catalyst on the metal oxide surface in proximity of the sensitizer promotes a more efficient electronic communication between the catalyst and the oxidized chromophore. Immobilization of the catalyst may also prevent oxidation of one catalyst by a neighboring catalyst in a highly oxidized form that could lead to decomposition of the active catalyst. In order to have fast electron transfer, an explored alternative is also the covalent binding of the metal catalyst center and the chromophore; the resulting dye/catalyst assembly is then grafted (through the chromophore anchoring) to the metal oxide surface [5]. As a matter of fact, despite substantial research efforts, the effective integration of dyes, catalysts, and semiconductors into efficient devices is still a challenge and only few complete systems have been reported so far [180]. The first assembled molecular photoanode was reported

in 2009 by Mollouk and co-workers [181], employing a bifunctional heteroleptic Ru(II) sensitizer (hereafter termed dye1), showing phosphonate groups for TiO_2 anchoring, and a malonate group to bind to hydrated iridium oxide ($IrO_2 \cdot nH_2O$) nanoparticle. Under light irradiation, this type of DSPEC produced both oxygen and hydrogen, even if poor internal quantum yield and coulombic efficiency (about 0.9% and 20%, respectively) were reported [181]. The low performances were mainly attributed to a slow hole transfer from the oxidized dye to the catalyst which, in turn, favored a high back recombination from TiO_2 to the oxidized dye. A fast dye's excited state quenching by $IrO_2 \cdot nH_2O$ has also been envisioned [182] as a possible additional deactivation channel. Here we review the recent modeling study [68] of the interfacial energetics and charge separation properties of the TiO_2/dye1/IrO_2 Mallouk's photoanode (Figure 8 top panel). The electronic structure of the TiO_2/dye1 interface (Figure 8 bottom panel) presents three almost degenerate HOMOs mainly localized on the dye. A significant broadening of the dye LUMO is calculated, which extends ~0.5 eV above the energy of the TiO_2 CB bottom over a range of ~2 eV. This picture is suggestive of strongly coupled electronic states, inducing fast electron injection. When dye1 is bound to the IrO_2 nanoparticle, three almost pure dye HOMOs are recognizable ~0.6–0.7 eV below the IrO_2 VB edge. This energy difference represents the maximum driving force for hole injection into IrO_2. The reduced interaction between the dye1 HOMOs and the IrO_2 VB, as inferred by the negligible HOMOs broadening in the dye-IrO_2 assembly, is an indication of the weak electronic coupling associated to the dye $\rightarrow$ IrO_2 hole transfer process [181]. The dye LUMO broadening upon interaction with the IrO_2 CB states, even if considerably weaker than that observed in the TiO_2-dye assembly, is still appreciable. This latter data is in line with the measured efficient excited state quenching observed for IrO_2-bound sensitizers [182].
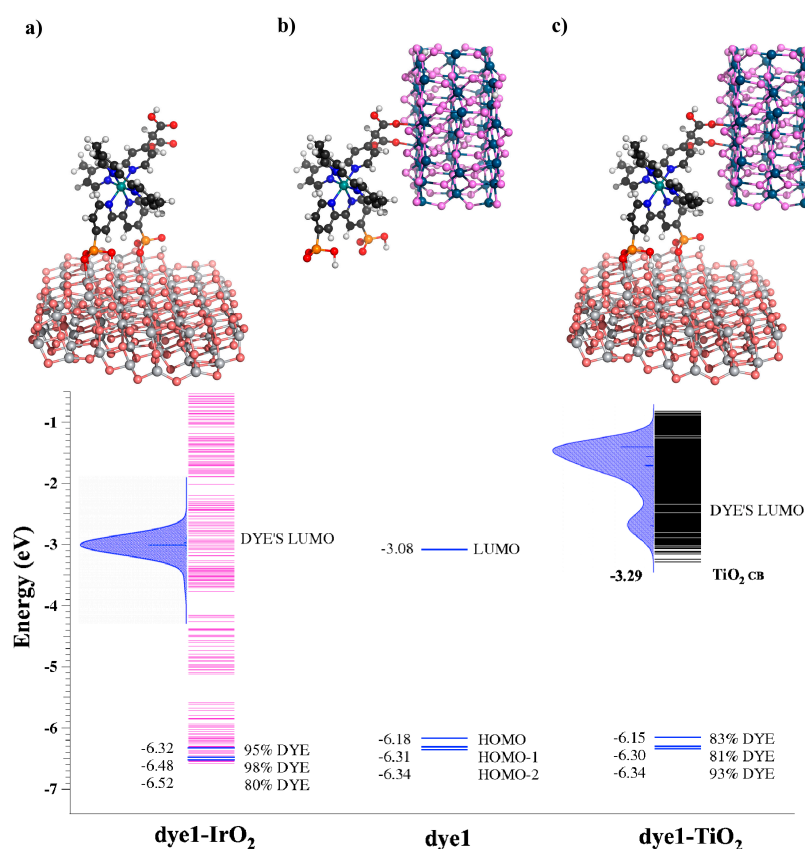

Figure 8. (**top**) Optimized molecular structure of the dye/TiO_2 (**a**); dye/IrO_2 (**b**); and TiO_2/dye/IrO_2 (**c**) assemblies; (**bottom**) alignment of energy levels for dye1 at TiO_2/dye and dye/IrO_2 interfaces compared to the energy levels of the stand-alone dye. Dye, IrO_2 and TiO_2 levels are in blue, magenta, and black colors, respectively. The percentages of dye contributions to the HOMOs of TiO_2/dye and dye/IrO_2 assemblies are also reported. Figure adapted from [68].

The calculated rates of the relevant interfacial electron and holes transfer processes are reported in Table 4 Here, we briefly point out that under the weak coupling assumption, the rate constant (k_{inj}) for the electron transfer from a single sensitizer's d state to the acceptor states k of the semiconductor can be expressed using the Fermi Golden Rule through the relation:

$$K_{inj} = \frac{2\pi}{\hbar} \sum_k |V_{dk}|^2 \rho(\varepsilon_k) \tag{1}$$

where $\rho(\varepsilon_k)$ is the density of semiconductor acceptor states (DOS) at the energy ε_k, V_{dk} is the electronic coupling matrix element between the diabatic donor d state and the k_{th} acceptor state in TiO$_2$ and $\hbar$ is Planck's constant. The $|V_{dk}|^2\rho(\varepsilon_k)$ product is the probability distribution $\Gamma(\varepsilon_k)$. The inverse of k_{inj} is the injection time τ. To calculate the electronic coupling elements, here use is made of the model recently developed by Thoss et al. [81] and based on a full diabatization of the problem by means of the localization of the molecular orbitals of the complex on the donor (chromophore) and acceptor (semiconductor) moieties. This provide the diabatic semiconductor DOS and the diabatic dye's LUMO, as well as the explicit coupling between the dye's LUMO and the manifold of the semiconductor empty states. Table 4 compiles the $\Gamma(\varepsilon)$, DOS and electron injection rates, τ (fs), and values extracted at the diabatic dye HOMO/LUMO values. As is apparent, the fastest process (highest k) is the electron injection from the dye LUMO to the TiO$_2$ CB, which is predicted to occur on the fs time scale, in agreement with the experimental <100 fs dynamics observed for this process [183] The hole injection from the dye HOMO to the IrO$_2$ VB is about three orders of magnitude less efficient. The rate of the parasitic oxidative dye excited state quenching to IrO$_2$ is comparable to that of hole injection. Notably, in agreement with the ms experimental time scale reported [181] recombination to the oxidized dye is calculated to be an extremely slow process, due to the negligible energetic overlap between the dye HOMO and the TiO$_2$ CB (poor DOS of acceptor states). Therefore, the quantitative picture extracted from our calculations clearly highlights the problems associated with the functioning of the DSPEC reported by Mollouk and co-workers [181], i.e., despite a typically fast electron injection into TiO$_2$, a slow hole injection into IrO$_2$ and a comparable rate of IrO$_2$ reduction by the photoexcited dye are indeed predicted.

Table 4. Probability distributions, $\Gamma(\varepsilon)$ (eV), and DOS (number of states/eV) calculated at the diabatic HOMO and LUMO energies, and associated injection rates, k_{inj} (s^{-1}).

System	Γ (eV)	DOS (States/eV)	k_{inj} (s^{-1})
Dye* + TiO$_2$ → Dye$^+$ + TiO$_2$ (e$^-$)			
dye1-TiO$_2$	0.1128	106	1.6×10^{14}
Dye* + IrO$_2$ → Dye$^+$ + IrO$_2$ (e$^-$)			
dye1-IrO$_2$	2.5×10^{-4}	37	3.3×10^{11}
IrO$_2$ + Dye (h$^+$) → IrO$_2$ (h$^+$) + Dye			
dye1-IrO$_2$	4.5×10^{-4}	48	1.0×10^{12}
TiO$_2$-dye1-IrO$_2$	2.7×10^{-4}	45	0.5×10^{11}
TiO$_2$ (e$^-$) + Dye (h$^+$) → TiO$_2$ + Dye			
dye1-TiO$_2$	6.3×10^{-11}	1.5×10^{-9}	1.0×10^4

5. Conclusions

Computational modelling of complex systems, such as dye-sensitized metal oxides surfaces, has seen a tremendous expansion in the last few years thanks to the excellent compromise between accuracy and computational cost reached by modern DFT and TDDFT methodologies. The calculation of redox and optical properties of standalone sensitizers is nowadays ordinary at DFT/TDDFT level and it is becoming affordable also for correlated ab initio methodologies, which however present the problem of properly dealing with a high number of excited states of different charge separation character.

Concerning the interface, the limitations of DFT/TDDFT for the description of organic dye/sensitized metal oxides come for the well-known difficulties of TDDFT in describing charge-transfer excited states. The use of GW and GW-BSE methods offer solutions to these shortcomings, delivering accurate results for isolated dyes and reliable description of the dye/TiO_2 interfacial energetics and optical properties, respectively. The computational overhead for GW-based calculations is at the moment the main limitation in its extensive application to realistic complex interfaces. We have also discussed how the computational modelling framework developed in the last years for the DSCs can be successfully extended to describe multiple metal oxide/dye/catalyst interfaces for water oxidation. Quantitative analysis of the electron and hole transfer rates based on extended photoanode models, has been shown to unveil the electronic features underlying the device functioning, opening, *de facto*, the way to a computationally-driven design of more efficient materials. Full atomistic understanding of the DSPECs is, however, still a challenge. The necessity of developing reliable models able to account for dynamical and environmental effects, charge separation dynamics, and redox properties along the reaction pathways is, nowadays, the most compelling challenge in this research area.

Conflicts of Interest: The author declares no conflict of interest.

References

1. Lewis, N.S.; Nocera, D.G. Powering the Planet: Chemical Challenges in Solar Energy Utilization. *Proc. Natl. Acad. Sci. USA* **2006**, *103*, 15729–15735. [CrossRef] [PubMed]
2. Armaroli, N.; Balzani, V. Solar Electricity and Solar Fuels: Status and Perspectives in the Context of the Energy Transition. *Chem. Eur. J.* **2016**, *22*, 32–57. [CrossRef] [PubMed]
3. Service, R.F. Is It Time to Shoot for the Sun? *Science* **2005**, *309*, 548–551. [CrossRef] [PubMed]
4. Nocera, D.G. On the Future of Global Energy. *Daedalus* **2006**, *135*, 112–115. [CrossRef]
5. Young, K.J.; Martini, L.A.; Milot, R.L.; Snoeberger, R.C., III; Batista, V.S.; Schmuttenmaer, C.A.; Crabtree, R.H.; Brudvig, G.W. Light-Driven Water Oxidation for Solar Fuels. *Coord. Chem. Rev.* **2012**, *256*, 2503–2520. [CrossRef] [PubMed]
6. Hamann, T.W. Water Splitting: An Adaptive Junction. *Nat. Mater.* **2014**, *13*, 3–4. [CrossRef] [PubMed]
7. Concepcion, J.J.; House, R.L.; Papanikolas, J.M.; Meyer, T.J. Chemical Approaches to Artificial Photosynthesis. *Proc. Natl. Acad. Sci. USA* **2012**, *109*, 15560–15564. [CrossRef] [PubMed]
8. Porter, G. Criteria for Solar Energy Conversion. In *Light, Chemical Change and Life. A Source Book in Photochemistry*; Coyle, J.D., Hill, R.R., Roberts, D.R., Eds.; Open University Press: Milton Keynes, UK, 1982; pp. 338–345.
9. O'Regan, B.; Grätzel, M. A Low-Cost, High-Efficiency Solar Cell Based on Dye-Sensitized Colloidal TiO_2 Films. *Nature* **1991**, *353*, 737–740. [CrossRef]
10. Grätzel, M. Photoelectrochemical Cells. *Nature* **2001**, *414*, 338–344. [CrossRef] [PubMed]
11. Walter, M.G.; Warren, E.L.; McKone, J.R.; Boettcher, S.W.; Mi, Q.; Santori, E.A.; Lewis, N.S. Solar Water Splitting Cells. *Chem. Rev.* **2010**, *110*, 6446–6473. [CrossRef] [PubMed]
12. Alibabaei, L.; Brennaman, M.K.; Norris, M.R.; Kalanyan, B.; Song, W.; Losego, M.D.; Concepcion, J.J.; Binstead, R.A.; Parsons, G.N.; Meyer, T.J. Solar Water Splitting in a Molecular Photoelectrochemical Cell. *Proc. Natl. Acad. Sci. USA* **2013**, *110*, 20008–20013. [CrossRef] [PubMed]
13. Boschloo, G.; Hagfeldt, A. Characteristics of the Iodide/Triiodide Redox Mediator in Dye-Sensitized Solar Cells. *Acc. Chem. Res.* **2009**, *42*, 1819–1826. [CrossRef] [PubMed]
14. Hagfeldt, A.; Boschloo, G.; Sun, L.; Kloo, L.; Pettersson, H. Dye-Sensitized Solar Cells. *Chem. Rev.* **2010**, *110*, 6595–6663. [CrossRef] [PubMed]
15. O'Regan, B.C.; Durrant, J.R. Kinetic and Energetic Paradigms for Dye-Sensitized Solar Cells: Moving from the Ideal to the Real. *Acc. Chem. Res.* **2009**, *42*, 1799–1808. [CrossRef] [PubMed]
16. Pastore, M.; Etienne, T.; De Angelis, F. Structural and Electronic Properties of Dye-Sensitized TiO_2 for Solar Cell Applications: From Single Molecules to Self-Assembled Monolayers. *J. Mater. Chem. C* **2016**, *4*, 4346–4373.
17. Li, L.-L.; Diau, E.W.-G. Porphyrin-Sensitized Solar Cells. *Chem. Soc. Rev.* **2013**, *42*, 291–304. [CrossRef] [PubMed]
18. Clifford, J.N.; Martinez-Ferrero, E.; Viterisi, A.; Palomares, E. Sensitizer Molecular Structure-Device Efficiency Relationship in Dye Sensitized Solar Cells. *Chem. Soc. Rev.* **2011**, *40*, 1635–1646. [CrossRef] [PubMed]

19. Ahmad, S.; Guillen, E.; Kavan, L.; Gratzel, M.; Nazeeruddin, M.K. Metal Free Sensitizer and Catalyst for Dye Sensitized Solar Cells. *Energy Environ. Sci.* **2013**, *6*, 3439–3466. [CrossRef]

20. Bozic-Weber, B.; Constable, E.C.; Housecroft, C.E. Light Harvesting with Earth Abundant D-Block Metals: Development of Sensitizers in Dye-Sensitized Solar Cells (Dscs). *Coord. Chem. Rev.* **2013**, *257*, 3089–3106. [CrossRef]

21. Imahori, H.; Umeyama, T.; Ito, S. Large Π-Aromatic Molecules as Potential Sensitizers for Highly Efficient Dye-Sensitized Solar Cells. *Acc. Chem. Res.* **2009**, *42*, 1809–1818. [CrossRef] [PubMed]

22. Xu, C.; Wu, J.; Desai, U.V.; Gao, D. High-Efficiency Solid-State Dye-Sensitized Solar Cells Based on TiO_2-Coated Zno Nanowire Arrays. *Nano Lett.* **2012**, *12*, 2420–2424. [CrossRef] [PubMed]

23. Wang, X.; Li, Z.; Shi, J.; Yu, Y. One-Dimensional Titanium Dioxide Nanomaterials: Nanowires, Nanorods, and Nanobelts. *Chem. Rev.* **2014**, *114*, 9346–9384. [CrossRef] [PubMed]

24. Wang, M.; Grätzel, C.; Zakeeruddin, S.M.; Grätzel, M. Recent Developments in Redox Electrolytes for Dye-Sensitized Solar Cells. *Energy Environ. Sci.* **2012**, *5*, 9394–9405. [CrossRef]

25. Wu, J.; Lan, Z.; Lin, J.; Huang, M.; Huang, Y.; Fan, L.; Luo, G. Electrolytes in Dye-Sensitized Solar Cells. *Chem. Rev.* **2015**, *115*, 2136–2173. [CrossRef] [PubMed]

26. Rüttinger, W.; Dismukes, G.C. Synthetic Water-Oxidation Catalysts for Artificial Photosynthetic Water Oxidation. *Chem. Rev.* **1997**, *97*, 1–24. [CrossRef] [PubMed]

27. Esswein, A.J.; Nocera, D.G. Hydrogen Production by Molecular Photocatalysis. *Chem. Rev.* **2007**, *107*, 4022–4047. [CrossRef] [PubMed]

28. Du, P.; Eisenberg, R. Catalysts Made of Earth-Abundant Elements (Co, Ni, Fe) for Water Splitting: Recent Progress and Future Challenges. *Energy Environ. Sci.* **2012**, *5*, 6012–6021. [CrossRef]

29. Yu, Z.; Li, F.; Sun, L. Recent Advances in Dye-Sensitized Photoelectrochemical Cells for Solar Hydrogen Production Based on Molecular Components. *Energy Environ. Sci.* **2015**, *8*, 760–775. [CrossRef]

30. Hardin, B.E.; Snaith, H.J.; McGehee, M.D. The Renaissance of Dye-Sensitized Solar Cells. *Nat. Photonics* **2012**, *6*, 162. [CrossRef]

31. Yen, Y.-S.; Chou, H.-H.; Chen, Y.-C.; Hsu, C.-Y.; Lin, J.T. Recent Developments in Molecule-Based Organic Materials for Dye-Sensitized Solar Cells. *J. Mater. Chem.* **2012**, *22*, 8734–8747. [CrossRef]

32. Coutard, N.; Kaeffer, N.; Artero, V. Molecular Engineered Nanomaterials for Catalytic Hydrogen Evolution and Oxidation. *Chem. Commun.* **2016**, *52*, 13728–13748. [CrossRef] [PubMed]

33. Brennaman, M.K.; Dillon, R.J.; Alibabaei, L.; Gish, M.K.; Dares, C.J.; Ashford, D.L.; House, R.L.; Meyer, G.J.; Papanikolas, J.M.; Meyer, T.J. Finding the Way to Solar Fuels with Dye-Sensitized Photoelectrosynthesis Cells. *J. Am. Chem. Soc.* **2016**, *138*, 13085–13102. [CrossRef] [PubMed]

34. Bazzan, G.; Deneault, J.R.; Kang, T.-S.; Taylor, B.E.; Durstock, M.F. Nanoparticle/Dye Interface Optimization in Dye-Sensitized Solar Cells. *Adv. Funct. Mater.* **2011**, *21*, 3268–3274. [CrossRef]

35. Cao, Y.; Cai, N.; Wang, Y.; Li, R.; Yuan, Y.; Wang, P. Modulating the Assembly of Organic Dye Molecules on Titania Nanocrystals Via Alkyl Chain Elongation for Efficient Mesoscopic Cobalt Solar Cells. *Phys. Chem. Chem. Phys.* **2012**, *14*, 8282–8286. [CrossRef] [PubMed]

36. Johansson, V.; Ellis-Gibbings, L.; Clarke, T.; Gorlov, M.; Andersson, G.G.; Kloo, L. On the Correlation between Dye Coverage and Photoelectrochemical Performance in Dye-Sensitized Solar Cells. *Phys. Chem. Chem. Phys.* **2014**, *16*, 711–718. [CrossRef] [PubMed]

37. Pazoki, M.; Lohse, P.W.; Taghavinia, N.; Hagfeldt, A.; Boschloo, G. The Effect of Dye Coverage on the Performance of Dye-Sensitized Solar Cells with a Cobalt-Based Electrolyte. *Phys. Chem. Chem. Phys.* **2014**, *16*, 8503–8508. [CrossRef] [PubMed]

38. Mahanta, S.; Matsuzaki, H.; Murakami, T.N.; Katoh, R.; Matsumoto, H.; Furube, A. Modulation of Electron Injection Dynamics of Ru-Based Dye/TiO_2 System in the Presence of Three Different Organic Solvents: Role of Solvent Dipole Moment and Donor Number. *ChemPhysChem* **2015**, *16*, 1657–1662. [CrossRef] [PubMed]

39. Agrawal, S.; Leijtens, T.; Ronca, E.; Pastore, M.; Snaith, H.; De Angelis, F. Modeling the Effect of Ionic Additives on the Optical and Electronic Properties of a Dye-Sensitized TiO_2 Heterointerface: Absorption, Charge Injection and Aggregation. *J. Mater. Chem. A* **2013**, *1*, 14675–14685. [CrossRef]

40. Marotta, G.; Reddy, M.A.; Singh, S.P.; Islam, A.; Han, L.; De Angelis, F.; Pastore, M.; Chandrasekharam, M. Novel Carbazole-Phenothiazine Dyads for Dye-Sensitized Solar Cells: A Combined Experimental and Theoretical Study. *ACS Appl. Mater. Interfaces* **2013**, *5*, 9635–9647. [CrossRef] [PubMed]

41. Gupta, K.S.V.; Zhang, J.; Marotta, G.; Reddy, M.A.; Singh, S.P.; Islam, A.; Han, L.; De Angelis, F.; Chandrasekharam, M.; Pastore, M. Effect of the Anchoring Group in the Performance of Carbazole-Phenothiazine Dyads for Dye-Sensitized Solar Cells. *Dyes Pigment.* **2015**, *113*, 536–545. [CrossRef]

42. Vaissier, V.; Frost, J.M.; Barnes, P.R.F.; Nelson, J. Influence of Intermolecular Interactions on the Reorganization Energy of Charge Transfer between Surface-Attached Dye Molecules. *J. Phys. Chem. C* **2015**, *119*, 24337–24341. [CrossRef]

43. Pastore, M.; Fantacci, S.; De Angelis, F. Modeling Excited States and Alignment of Energy Levels in Dye-Sensitized Solar Cells: Successes, Failures, and Challenges. *J. Phys. Chem. C* **2013**, *117*, 3685–3700. [CrossRef]

44. Pastore, M.; Fantacci, S.; De Angelis, F. Ab Initio Determination of Ground and Excited State Oxidation Potentials of Organic Chromophores for Dye-Sensitized Solar Cells. *J. Phys. Chem. C* **2010**, *114*, 22742–22750. [CrossRef]

45. Pastore, M.; Mosconi, E.; De Angelis, F. Computational Investigation of Dye-Iodine Interactions in Organic Dye-Sensitized Solar Cells. *J. Phys. Chem. C* **2012**, *116*, 5965–5973. [CrossRef]

46. Labat, F.; Le Bahers, T.; Ciofini, I.; Adamo, C. First-Principles Modeling of Dye-Sensitized Solar Cells: Challenges and Perspectives. *Acc. Chem. Res.* **2012**, *45*, 1268–1277. [CrossRef] [PubMed]

47. Labat, F.; Ciofini, I.; Hratchian, H.P.; Frisch, M.J.; Raghavachari, K.; Adamo, C. Insights into Working Principles of Ruthenium Polypyridyl Dye-Sensitized Solar Cells from First Principles Modeling. *J. Phys. Chem. C* **2011**, *115*, 4297–4306. [CrossRef]

48. Martsinovich, N.; Troisi, A. Theoretical Studies of Dye-Sensitised Solar Cells: From Electronic Structure to Elementary Processes. *Energy Environ. Sci.* **2011**, *4*, 4473–4495. [CrossRef]

49. Martsinovich, N.; Troisi, A. High-Throughput Computational Screening of Chromophores for Dye-Sensitized Solar Cells. *J. Phys. Chem. C* **2011**, *115*, 11781–11792. [CrossRef]

50. Martsinovich, N.; Ambrosio, F.; Troisi, A. Adsorption and Electron Injection of the N3 Metal-Organic Dye on the TiO_2 Rutile (110) Surface. *Phys. Chem. Chem. Phys.* **2012**, *14*, 16668–16676. [CrossRef] [PubMed]

51. Fantacci, S.; De Angelis, F.; Selloni, A. Absorption Spectrum and Solvatochromism of the $[Ru(4,4'-Cooh-2,2'-Bpy)_2(Ncs)_2]$ Molecular Dye by Time Dependent Density Functional Theory. *J. Am. Chem. Soc.* **2003**, *125*, 4381–4387. [CrossRef] [PubMed]

52. Nazeeruddin, M.K.; De Angelis, F.; Fantacci, S.; Selloni, A.; Viscardi, G.; Liska, P.; Ito, S.; Takeru, B.; Grätzel, M. Combined Experimental and DFT-TDDFT Computational Study of Photoelectrochemical Cell Ruthenium Sensitizers. *J. Am. Chem. Soc.* **2005**, *127*, 16835–16847. [CrossRef] [PubMed]

53. Fantacci, S.; De Angelis, F.; Nazeeruddin, M.K.; Grätzel, M. Electronic and Optical Properties of the Spiro-Meotad Hole Conductor in Its Neutral and Oxidized Forms: A DFT/TDDFT Investigation. *J. Phys. Chem. C* **2011**, *115*, 23126–23133. [CrossRef]

54. Jacquemin, D.; Perpète, E.A.; Ciofini, I.; Adamo, C. Accurate Simulation of Optical Properties in Dyes. *Acc. Chem. Res.* **2009**, *42*, 326–334. [CrossRef] [PubMed]

55. Jacquemin, D.; Perpete, E.A.; Scuseria, G.E.; Ciofini, I.; Adamo, C. TD-DFT Performance for the Visible Absorption Spectra of Organic Dyes: Conventional Versus Long-Range Hybrids. *J. Chem. Theor.Comp.* **2008**, *4*, 123–135. [CrossRef] [PubMed]

56. Ertem, M.Z.; Gagliardi, L.; Cramer, C.J. Quantum Chemical Characterization of the Mechanism of an Iron-Based Water Oxidation Catalyst. *Chem. Sci.* **2012**, *3*, 1293–1299. [CrossRef]

57. Mavros, M.G.; Tsuchimochi, T.; Kowalczyk, T.; McIsaac, A.; Wang, L.-P.; Voorhis, T.V. What Can Density Functional Theory Tell Us about Artificial Catalytic Water Splitting? *Inorg. Chem.* **2014**, *53*, 6386–6397. [CrossRef] [PubMed]

58. Ping, Y.; Rocca, D.; Galli, G. Electronic Excitations in Light Absorbers for Photoelectrochemical Energy Conversion: First Principles Calculations Based on Many Body Perturbation Theory. *Chem. Soc. Rev.* **2013**, *42*, 2437–2469. [CrossRef] [PubMed]

59. Pastore, M.; De Angelis, F.; Angeli, C. Optical Absorption Spectrum of the N3 Solar Cell Sensitizer by Second-Order Multireference Perturbation Theory. *Theor. Chem. Acc.* **2016**, *135*, 1–11. [CrossRef]

60. Chen, P.; Yum, J.H.; De Angelis, F.; Mosconi, E.; Fantacci, S.; Moon, S.-J.; Baker, R.H.; Ko, J.; Nazeeruddin, M.K.; Grätzel, M. High Open-Circuit Voltage Solid-State Dye-Sensitized Solar Cells with Organic Dye. *Nano Lett.* **2009**, *9*, 2487–2492. [CrossRef] [PubMed]

61. De Angelis, F.; Fantacci, S.; Selloni, A.; Grätzel, M.; Nazeeruddin, M.K. Influence of the Sensitizer Adsorption Mode on the Open-Circuit Potential of Dye-Sensitized Solar Cells. *Nano Lett.* **2007**, *7*, 3189–3195. [CrossRef] [PubMed]

62. Pastore, M.; Selloni, A.; Fantacci, S.; De Angelis, F. Electronic and Optical Properties of Dye-Sensitized TiO$_2$ Interfaces. In *First Principles Approaches to Spectroscopic Properties of Complex Materials*; Springer: Berlin/Heidelberg, Germany, 2014; pp. 1–45.

63. Maggio, E.; Martsinovich, N.; Troisi, A. Theoretical Study of Charge Recombination at the TiO$_2$-Electrolyte Interface in Dye Sensitised Solar Cells. *J. Chem. Phys.* **2012**, *137*, 22A508. [CrossRef] [PubMed]

64. Ambrosio, F.; Martsinovich, N.; Troisi, A. What Is the Best Anchoring Group for a Dye in a Dye-Sensitized Solar Cell? *J. Phys. Chem. Lett.* **2012**, *3*, 1531–1535. [CrossRef] [PubMed]

65. Labat, F.; Ciofini, I.; Adamo, C. Revisiting the Importance of Dye Binding Mode in Dye-Sensitized Solar Cells: A Periodic Viewpoint. *J. Mater. Chem.* **2012**, *22*, 12205–12211. [CrossRef]

66. Jakubikova, E.; Snoeberger Iii, R.C.; Batista, V.S.; Martin, R.L.; Batista, E.R. Interfacial Electron Transfer in TiO$_2$ Surfaces Sensitized with Ru(Ii)−Polypyridine Complexes. *J. Phys. Chem. A* **2009**, *113*, 12532–12540. [CrossRef] [PubMed]

67. Li, G.; Sproviero, E.M.; Snoeberger Iii, R.C.; Iguchi, N.; Blakemore, J.D.; Crabtree, R.H.; Brudvig, G.W.; Batista, V.S. Deposition of an Oxomanganese Water Oxidation Catalyst on TiO$_2$ Nanoparticles: Computational Modeling, Assembly and Characterization. *Energy Environ. Sci.* **2009**, *2*, 230–238. [CrossRef]

68. Pastore, M.; De Angelis, F. First-Principles Modeling of a Dye-Sensitized TiO$_2$/IrO$_2$ Photoanode for Water Oxidation. *J. Am. Chem. Soc.* **2015**, *137*, 5798–5809. [CrossRef] [PubMed]

69. Rego, L.G.C.; Batista, V.S. Quantum Dynamics Simulations of Interfacial Electron Transfer in Sensitized TiO$_2$ Semiconductors. *J. Am. Chem. Soc.* **2003**, *125*, 7989–7997. [CrossRef] [PubMed]

70. Negre, C.F.A.; Milot, R.L.; Martini, L.A.; Ding, W.; Crabtree, R.H.; Schmuttenmaer, C.A.; Batista, V.S. Efficiency of Interfacial Electron Transfer from Zn-Porphyrin Dyes into TiO$_2$ Correlated to the Linker Single Molecule Conductance. *J. Phys. Chem. C* **2013**, *117*, 24462–24470. [CrossRef]

71. Sproviero, E.M.; Shinopoulos, K.; Gascón, J.A.; McEvoy, J.P.; Brudvig, G.W.; Batista, V.S. Qm/Mm Computational Studies of Substrate Water Binding to the Oxygen-Evolving Centre of Photosystem II. *Philos. Trans. R. Soc. B Biol. Sci.* **2008**, *363*, 1149–1156. [CrossRef] [PubMed]

72. Monti, A.; de Ruiter, J.M.; de Groot, H.J.M.; Buda, F. A Dynamic View of Proton-Coupled Electron Transfer in Photocatalytic Water Splitting. *J. Phys. Chem. C* **2016**, *120*, 23074–23082. [CrossRef]

73. Sulzer, D.; Iuchi, S.; Yasuda, K. A New Method to Evaluate Excited States Lifetimes Based on Green's Function: Application to Dye-Sensitized Solar Cells. *J. Chem. Theor. Comp.* **2016**, *12*, 3074–3086. [CrossRef] [PubMed]

74. Umari, P.; Giacomazzi, L.; De Angelis, F.; Pastore, M.; Baroni, S. Energy-Level Alignment in Organic Dye-Sensitized TiO$_2$ from GW Calculations. *J. Chem. Phys.* **2013**, *139*, 014709. [CrossRef] [PubMed]

75. Munoz-Garcia, A.B.; Pavone, M. Structure and Energy Level Alignment at the Dye-Electrode Interface in P-Type Dsscs: New Hints on the Role of Anchoring Modes from Ab Initio Calculations. *Phy. Chem. Chem. Phys.* **2015**, *17*, 12238–12246. [CrossRef] [PubMed]

76. Kontkanen, O.V.; Niskanen, M.; Hukka, T.I.; Rantala, T.T. Electronic Structure of P-Type Perylene Monoimide-Based Donor-Acceptor Dyes on the Nickel Oxide (100) Surface: A DFT Approach. *Phys. Chem. Chem. Phys.* **2016**, *18*, 14382–14389. [CrossRef] [PubMed]

77. Chen, K.J.; Laurent, A.D.; Boucher, F.; Odobel, F.; Jacquemin, D. Determining the Most Promising Anchors for Cuscn: Ab Initio Insights Towards P-Type Dsscs. *J. Mater. Chem. A* **2016**, *4*, 2217–2227. [CrossRef]

78. Pastore, M.; Duchanois, T.; Liu, L.; Monari, A.; Assfeld, X.; Haacke, S.; Gros, P.C. Interfacial Charge Separation and Photovoltaic Efficiency in Fe(II)-Carbene Sensitized Solar Cells. *Phys. Chem. Chem. Phys.* **2016**, *18*, 28069–28081. [CrossRef] [PubMed]

79. Salvatori, P.; Amat, A.; Pastore, M.; Vitillaro, G.; Sudhakar, K.; Giribabu, L.; Soujanya, Y.; De Angelis, F. Corrole Dyes for Dye-Sensitized Solar Cells: The Crucial Role of the Dye/Semiconductor Energy Level Alignment. *Comp. Theor. Chem.* **2014**, *1030*, 59–66. [CrossRef]

80. Stier, W.; Prezhdo, O.V. Nonadiabatic Molecular Dynamics Simulation of Light-Induced Electron Transfer from an Anchored Molecular Electron Donor to a Semiconductor Acceptor. *J. Phys. Chem. B* **2002**, *106*, 8047–8054. [CrossRef]

81. Kondov, I.; Čížek, M.; Benesch, C.; Wang, H.; Thoss, M. Quantum Dynamics of Photoinduced Electron-Transfer Reactions in Dye-Semiconductor Systems: First-Principles Description and Application to Coumarin 343−TiO_2. *J. Phys. Chem. C* **2007**, *111*, 11970–11981. [CrossRef]

82. Meng, S.; Ren, J.; Kaxiras, E. Natural Dyes Adsorbed on TiO_2 Nanowire for Photovoltaic Applications: Enhanced Light Absorption and Ultrafast Electron Injection. *Nano Lett.* **2008**, *8*, 3266–3272. [CrossRef] [PubMed]

83. Monti, A.; Negre, C.F.A.; Batista, V.S.; Rego, L.G.C.; de Groot, H.J.M.; Buda, F. Crucial Role of Nuclear Dynamics for Electron Injection in a Dye-Semiconductor Complex. *J. Phys. Chem. Lett.* **2015**, *6*, 2393–2398. [CrossRef] [PubMed]

84. Pal, S.; Trivedi, D.J.; Akimov, A.V.; Aradi, B.; Frauenheim, T.; Prezhdo, O.V. Nonadiabatic Molecular Dynamics for Thousand Atom Systems: A Tight-Binding Approach toward Pyxaid. *J. Chem. Theor. Comp.* **2016**, *12*, 1436–1448. [CrossRef] [PubMed]

85. Abuabara, S.G.; Rego, L.G.C.; Batista, V.S. Influence of Thermal Fluctuations on Interfacial Electron Transfer in Functionalized TiO_2 Semiconductors. *J. Am. Chem. Soc.* **2005**, *127*, 18234–18242. [CrossRef] [PubMed]

86. Duncan, W.R.; Stier, W.M.; Prezhdo, O.V. Ab Initio Nonadiabatic Molecular Dynamics of the Ultrafast Electron Injection across the Alizarin-TiO_2 Interface. *J. Am. Chem. Soc.* **2005**, *127*, 7941–7951. [CrossRef] [PubMed]

87. Li, J.; Wang, H.; Persson, P.; Thoss, M. Photoinduced Electron Transfer Processes in Dye-Semiconductor Systems with Different Spacer Groups. *J. Chem. Phys.* **2012**, *137*, 22A529. [CrossRef] [PubMed]

88. Marques, M.A.L.; López, X.; Varsano, D.; Castro, A.; Rubio, A. Time-Dependent Density-Functional Approach for Biological Chromophores: The Case of the Green Fluorescent Protein. *Phys. Rev. Lett.* **2003**, *90*, 258101–258104. [CrossRef] [PubMed]

89. Meng, S.; Kaxiras, E. Electron and Hole Dynamics in Dye-Sensitized Solar Cells: Influencing Factors and Systematic Trends. *Nano Lett.* **2010**, *10*, 1238–1247. [CrossRef] [PubMed]

90. Angeli, C.; Pastore, M.; Cimiraglia, C. New Perspectives in Multireference Perturbation Theory: The N-Electron Valence State Approach. *Theor. Chem. Acc.* **2007**, *117*, 743–754. [CrossRef]

91. Angeli, C.; Cimiraglia, R.; Evangelisti, S.; Leininger, T.; Malrieu, J.-P. Introduction of N-Electron Valence States for Multireference Perturbation Theory. *J. Chem. Phys.* **2001**, *114*, 10252–10264. [CrossRef]

92. Angeli, C.; Cimiraglia, R.; Malrieu, J.-P. N-Electron Valence State Perturbation Theory: A Fast Implementation of the Strongly Contracted Variant. *Chem. Phys. Lett.* **2001**, *350*, 297–305. [CrossRef]

93. Neese, F. The Orca Program System. *WIREs Comp. Mol. Sci.* **2012**, *2*, 73–78. [CrossRef]

94. Hedin, L. New Method for Calculating the One-Particle Green's Function with Application to the Electron-Gas Problem. *Phys. Rev.* **1965**, *139*, A796–A823. [CrossRef]

95. Hybertsen, M.S.; Louie, S.G. Electron Correlation in Semiconductors and Insulators: Band Gaps and Quasiparticle Energies. *Phys. Rev. B* **1986**, *34*, 5390–5413. [CrossRef]

96. Pastore, M.; Mosconi, E.; De Angelis, F.; Grätzel, M. A Computational Investigation of Organic Dyes for Dye-Sensitized Solar Cells: Benchmark, Strategies, and Open Issues. *J. Phys. Chem. C* **2010**, *114*, 7205–7212. [CrossRef]

97. Delgado, A.; Corni, S.; Goldoni, G. Low-Lying Electronic Excitations and Optical Absorption Spectra of the Black Dye Sensitizer: A First-Principles Study. *Theor. Chem. Acc.* **2012**, *131*, 1–14. [CrossRef]

98. Faber, C.; Duchemin, I.; Deutsch, T.; Blase, X. Many-Body Green's Function Study of Coumarins for Dye-Sensitized Solar Cells. *Phys. Rev. B* **2012**, *86*, 155315. [CrossRef]

99. Umari, P.; Mosconi, E.; De Angelis, F. Relativistic GW Calculations on $CH_3NH_3PbI_3$ and $CH_3NH_3SnI_3$ Perovskites for Solar Cell Applications. *Sci. Rep.* **2014**, *4*, 4467. [CrossRef] [PubMed]

100. Marom, N.; Moussa, J.E.; Ren, X.; Tkatchenko, A.; Chelikowsky, J.R. Electronic Structure of Dye-Sensitized TiO_2 Clusters from Many-Body Perturbation Theory. *Phys. Rev. B* **2011**, *84*, 245115. [CrossRef]

101. Sproviero, E.M.; Gascón, J.A.; McEvoy, J.P.; Brudvig, G.W.; Batista, V.S. Quantum Mechanics/Molecular Mechanics Study of the Catalytic Cycle of Water Splitting in Photosystem II. *J. Am. Chem. Soc.* **2008**, *130*, 3428–3442. [CrossRef] [PubMed]

102. Yang, X.; Hall, M.B. Mechanism of Water Splitting and Oxygen−Oxygen Bond Formation by a Mononuclear Ruthenium Complex. *J. Am. Chem. Soc.* **2009**, *132*, 120–130. [CrossRef] [PubMed]

103. Sobolewski, A.L.; Domcke, W. Computational Model of Photocatalytic Water Splitting. *J. Phys. Chem. A* **2008**, *112*, 7311–7313. [CrossRef] [PubMed]

104. Rivalta, I.; Brudvig, G.W.; Batista, V.S. Computational Studies of the Oxygen-Evolving Complex of Photosystem II and Biomimetic Oxomanganese Complexes for Renewable Energy Applications. In *Applications of Molecular Modeling to Challenges in Clean Energy*; American Chemical Society: Washington, DC, USA, 2013; Volume 1133, pp. 203–215.

105. Pastore, M.; Mosconi, E.; Fantacci, S.; De Angelis, F. Computational Investigations on Organic Sensitizers for Dye- Sensitized Solar Cells. *Curr. Org. Synth.* **2012**, *9*, 215–232. [CrossRef]

106. Tognetti, V.; Joubert, L. Unraveling Charge Transfer Processes with the Quantum Theory of Atoms-in-Molecules. *Theor. Chem. Acc.* **2016**, *135*, 124. [CrossRef]

107. Ronca, E.; Angeli, C.; Belpassi, L.; De Angelis, F.; Tarantelli, F.; Pastore, M. Density Relaxation in Time-Dependent Density Functional Theory: Combining Relaxed Density Natural Orbitals and Multireference Perturbation Theories for an Improved Description of Excited States. *J. Chem. Theor. Comp.* **2014**, *10*, 4014–4024. [CrossRef] [PubMed]

108. Huang, S.; Zhang, Q.; Shiota, Y.; Nakagawa, T.; Kuwabara, K.; Yoshizawa, K.; Adachi, C. Computational Prediction for Singlet- and Triplet-Transition Energies of Charge-Transfer Compounds. *J. Chem. Theor. Comp.* **2013**, *9*, 3872–3877. [CrossRef] [PubMed]

109. Yanai, T.; Tew, D.P.; Handy, N.C. A New Hybrid Exchange-Correlation Functional Using the Coulomb-Attenuating Method (CAM-B3LYP). *Chem. Phys. Lett.* **2004**, *393*, 51–57. [CrossRef]

110. Baer, R.; Neuhauser, D. Density Functional Theory with Correct Long-Range Asymptotic Behavior. *Phys. Rev. Lett.* **2005**, *94*, 043002. [CrossRef] [PubMed]

111. Chai, J.-D.; Head-Gordon, M. Long-Range Corrected Hybrid Density Functionals with Damped Atom–Atom Dispersion Corrections. *Phys. Chem. Chem. Phys.* **2008**, *10*, 6615–6620. [CrossRef] [PubMed]

112. Vydrov, O.A.; Scuseria, G.E. Assessment of a Long-Range Corrected Hybrid Functional. *J. Chem. Phys.* **2006**, *125*, 234109. [CrossRef] [PubMed]

113. Rohrdanz, M.A.; Martins, K.M.; Herbert, J.M. A Long-Range-Corrected Density Functional That Performs Well for Both Ground-State Properties and Time-Dependent Density Functional Theory Excitation Energies, Including Charge-Transfer Excited States. *J. Chem. Phys.* **2009**, *130*, 054112. [CrossRef] [PubMed]

114. Baer, R.; Livshits, E.; Salzner, U. Tuned Range-Separated Hybrids in Density Functional Theory. *Annu. Rev. Phys. Chem.* **2010**, *61*, 85–109. [CrossRef] [PubMed]

115. Moore, B.; Charaf-Eddin, A.; Planchat, A.; Adamo, C.; Autschbach, J.; Jacquemin, D. Electronic Band Shapes Calculated with Optimally Tuned Range-Separated Hybrid Functionals. *J. Chem. Theor. Comp.* **2014**, *10*, 4599–4608. [CrossRef] [PubMed]

116. Kronik, L.; Stein, T.; Refaely-Abramson, S.; Baer, R. Excitation Gaps of Finite-Sized Systems from Optimally Tuned Range-Separated Hybrid Functionals. *J. Chem. Theor. Comp.* **2012**, *8*, 1515–1531. [CrossRef] [PubMed]

117. Sun, H.; Zhong, C.; Brédas, J.-L. Reliable Prediction with Tuned Range-Separated Functionals of the Singlet–Triplet Gap in Organic Emitters for Thermally Activated Delayed Fluorescence. *J. Chem. Theor. Comp.* **2015**, *11*, 3851–3858. [CrossRef] [PubMed]

118. Tortorella, S.; Talamo, M.M.; Cardone, A.; Pastore, M.; De Angelis, F. Benchmarking DFT and Semi-Empirical Methods for a Reliable and Cost-Efficient Computational Screening of Benzofulvene Derivatives as Donor Materials for Small-Molecule Organic Solar Cells. *J. Phys. Condens. Matter* **2016**, *28*, 074005. [CrossRef] [PubMed]

119. Kim, S.; Lee, J.K.; Kang, S.O.; Ko, J.; Yum, J.H.; Fantacci, S.; De Angelis, F.; Di Censo, D.; Nazeeruddin, M.K.; Grätzel, M. Molecular Engineering of Organic Sensitizers for Solar Cell Applications. *J. Am. Chem. Soc.* **2006**, *128*, 16701–16707. [CrossRef] [PubMed]

120. Schmidt-Mende, L.; Bach, U.; Humphry-Baker, R.; Horiuchi, T.; Miura, H.; Ito, S.; Uchida, S.; Grätzel, M. Organic Dye for Highly Efficient Solid-State Dye-Sensitized Solar Cells. *Adv. Mater.* **2005**, *17*, 813–815. [CrossRef]

121. Tomasi, J.; Mennucci, B.; Cammi, R. Quantum Mechanical Continuum Solvation Models. *Chem. Rev.* **2005**, *105*, 2999–3094. [CrossRef] [PubMed]

122. Azzaroli, N.; Lobello, M.G.; Lapini, A.; Iagatti, A.; Bussotti, L.; Di Donato, M.; Calogero, G.; Pastore, M.; De Angelis, F.; Foggi, P. Monitoring the Intramolecular Charge Transfer Process in the Z907 Solar Cell Sensitizer: A Transient Vis and Ir Spectroscopy and Ab Initio Investigation. *Phys. Chem. Chem. Phys.* **2015**, *17*, 21594–21604. [CrossRef] [PubMed]

123. Improta, R.; Barone, V. Absorption and Fluorescence Spectra of Uracil in the Gas Phase and in Aqueous Solution: A TD-DFT Quantum Mechanical Study. *J. Am. Chem. Soc.* **2004**, *126*, 14320–14321. [CrossRef] [PubMed]

124. Jacquemin, D.; Preat, J.; Wathelet, V.; Perpète, E.A. Substitution and Chemical Environment Effects on the Absorption Spectrum of Indigo. *J. Chem. Phys.* **2006**, *124*, 074104. [CrossRef] [PubMed]

125. Jacquemin, D.; Perpète, E.A.; Ciofini, I.; Adamo, C. On the TD-DFT UV/Vis Spectra Accuracy: The Azoalkanes. *Theor. Chem. Acc.* **2008**, *120*, 405–410. [CrossRef]

126. Umari, P.; Stenuit, G.; Baroni, S. GW Quasiparticle Spectra from Occupied States Only. *Phys. Rev. B* **2010**, *81*, 115104–115109. [CrossRef]

127. Umari, P.; Stenuit, G.; Baroni, S. Optimal Representation of the Polarization Propagator for Large-Scale GW Calculations. *Phys. Rev. B* **2009**, *79*, 201104. [CrossRef]

128. Giannozzi, P.; Baroni, S.; Bonini, N.; Calandra, M.; Car, R.; Cavazzoni, C.; Ceresoli, D.; Chiarotti, G.L.; Cococcioni, M.; Dabo, I.; et al. Quantum Espresso: A Modular and Open-Source Software Project for Quantum Simulations of Materials. *J. Phys. Condens. Matter* **2009**, *21*, 395502. [CrossRef] [PubMed]

129. Bruneval, F. GW Approximation of the Many-Body Problem and Changes in the Particle Number. *Phys. Rev. Lett.* **2009**, *103*, 176403. [CrossRef] [PubMed]

130. Körzdörfer, T.; Marom, N. Strategy for Finding a Reliable Starting Point for G_0W_0 Demonstrated for Molecules. *Phys. Rev. B* **2011**, *86*, 041110. [CrossRef]

131. Bruneval, F.; Marques, M.A.L. Benchmarking the Starting Points of the GW Approximation for Molecules. *J. Chem. Theor. Comp.* **2013**, *9*, 324–329. [CrossRef] [PubMed]

132. Jacquemin, D.; Duchemin, I.; Blase, X. Benchmarking the Bethe–Salpeter Formalism on a Standard Organic Molecular Set. *J. Chem. Theor. Comp.* **2015**, *11*, 3290–3304. [CrossRef] [PubMed]

133. Marinado, T.; Hagberg, D.; Hedlund, M.; Edvinsson, T.; Johansson, E.; Boschloo, G.; Rensmo, H.; Brinck, T.; Sun, L.; Hagfeldt, A. Rhodanine Dyes for Dye-Sensitized Solar Cells: Spectroscopy, Energy Levels and Photovoltaic Performance. *Phys. Chem. Chem. Phys.* **2009**, *11*, 133–141. [CrossRef] [PubMed]

134. Nazeeruddin, M.K.; Kay, A.; Rodicio, I.; Humphry-Baker, R.; Mueller, E.; Liska, P.; Vlachopoulos, N.; Graetzel, M. Conversion of Light to Electricity by Cis-X2bis(2,2′-Bipyridyl-4,4′-Dicarboxylate)Ruthenium(II) Charge-Transfer Sensitizers (X = Cl-, Br-, I-, CN-, and SCN-) on Nanocrystalline Titanium Dioxide Electrode. *J. Am. Chem. Soc.* **1993**, *115*, 6382–6390. [CrossRef]

135. Nazeeruddin, M.K.; Péchy, P.; Grätzel, M. Efficient Panchromatic Sensitization of Nanocrystalline TiO_2 Films by a Black Dye Based on Atrithiocyanato–Ruthenium Complex. *Chem. Commun.* **1997**, *18*, 1705–1706. [CrossRef]

136. Nazeeruddin, M.K.; Péchy, P.; Renouard, T.; Zakeeruddin, S.M.; Humphry-Baker, R.; Comte, P.; Liska, P.; Cevey, L.; Costa, E.; Shklover, V.; et al. Engineering of Efficient Panchromatic Sensitizers for Nanocrystalline TiO_2-Based Solar Cells. *J. Am. Chem. Soc.* **2001**, *123*, 1613–1624. [CrossRef] [PubMed]

137. Han, L.; Islam, A.; Chen, H.; Malapaka, C.; Chiranjeevi, B.; Zhang, S.; Yang, X.; Yanagida, M. High-Efficiency Dye-Sensitized Solar Cell with a Novel Co-Adsorbent. *Energy Environ. Sci.* **2012**, *5*, 6057–6060. [CrossRef]

138. Becke, A.D. A New Mixing of Hartree–Fock and Local Density-Functional Theories. *J. Chem. Phys.* **1993**, *98*, 1372–1377. [CrossRef]

139. Adamo, C.; Barone, V. Toward Reliable Density Functional Methods without Adjustable Parameters: The PBE0 Model. *J. Chem. Phys.* **1999**, *110*, 6158–6170. [CrossRef]

140. Zhao, Y.; Truhlar, D.G. The M06 Suite of Density Functionals for Main Group Thermochemistry, Thermochemical Kinetics, Noncovalent Interactions, Excited States, and Transition Elements: Two New Functionals and Systematic Testing of Four M06-Class Functionals and 12 Other Functionals. *Theor. Chem. Acc.* **2008**, *120*, 215–241.

141. De Angelis, F.; Fantacci, S.; Selloni, A. Time Dependent Density Functional Theory Study of the Absorption Spectrum of the $[Ru(4,4′-COO^−-2,2′-bpy)_2(X)_2]^{4−}$ (X = NCS, Cl) Dyes in Water Solution. *Chem. Phys. Lett.* **2005**, *415*, 115–120. [CrossRef]

142. De Angelis, F.; Fantacci, S.; Selloni, A. Time-Dependent Density Functional Theory Study of the Absorption Spectrum of $[Ru(4,4′-COOH-2,2′-bpy)_2(NCS)_2]$ in Water Solution: Influence of the pH. *Chem. Phys. Lett.* **2004**, *389*, 204–208. [CrossRef]

143. Monat, J.E.; Rodriguez, J.H.; McCusker, J.K. Ground- and Excited-State Electronic Structures of the Solar Cell Sensitizer Bis(4,4′-Dicarboxylato-2,2′-Bipyridine)Bis(Isothiocyanato)Ruthenium(II). *J. Phys. Chem. A* **2002**, *106*, 7399–7406. [CrossRef]

144. Jäger, M.; Freitag, L.; González, L. Using Computational Chemistry to Design Ru Photosensitizers with Directional Charge Transfer. *Coord. Chem. Rev.* **2015**, *304–305*, 146–165. [CrossRef]

145. Daniel, C. Photochemistry and Photophysics of Transition Metal Complexes: Quantum Chemistry. *Coord. Chem. Rev.* **2015**, *282–283*, 19–32. [CrossRef]

146. Piau, R.E.; Guillon, T.; Lebon, E.; Perrot, N.; Alary, F.; Boggio-Pasqua, M.; Heully, J.-L.; Juris, A.; Sutra, P.; Igau, A. Photophysical and Electrochemical Properties of Polypyridine Imine Ruthenium(II) Complexes: A Comparative Experimental and Theoretical Study. *New J. Chem.* **2012**, *36*, 2484–2492. [CrossRef]

147. Charlot, M.-F.; Aukauloo, A. Highlighting the Role of the Medium in DFT Analysis of the Photophysical Properties of Ruthenium(II) Polypyridine-Type Complexes. *J. Phys. Chem. A* **2007**, *111*, 11661–11672. [CrossRef] [PubMed]

148. Stoyanov, S.R.; Villegas, J.M.; Paul Rillema, D. The Charge Transfer Band Solvent-Dependence of [Ru(bpy)$_2$(CN$_x$)Cl]$^+$, CN$_x$ = 2,6-Dimethylphenylisocyanide: A Polarizable Continuum Model/Time-Dependent Density Functional Theory Study. *Inorg. Chem. Commun.* **2004**, *7*, 838–841. [CrossRef]

149. Fantacci, S.; De Angelis, F.; Sgamellotti, A.; Re, N. A Tddft Study of the Ruthenium(II) Polyazaaromatic Complex [Ru(dppz)(phen)$_2$]$^{2+}$ in Solution. *Chem. Phys. Lett.* **2004**, *396*, 43–48. [CrossRef]

150. Vlček, A., Jr.; Záliš, S. Modeling of Charge-Transfer Transitions and Excited States in D6 Transition Metal Complexes by DFT Techniques. *Coord. Chem. Rev.* **2007**, *251*, 258–287. [CrossRef]

151. Escudero, D.; González, L. Raspt2/Rasscf vs. Range-Separated/Hybrid DFT Methods: Assessing the Excited States of a Ru(II)Bipyridyl Complex. *J. Chem. Theor. Comp.* **2011**, *8*, 203–213. [CrossRef] [PubMed]

152. Chantzis, A.; Very, T.; Monari, A.; Assfeld, X. Improved Treatment of Surrounding Effects: UV/Vis Absorption Properties of a Solvated Ru(II) Complex. *J. Chem. Theor. Comp.* **2012**, *8*, 1536–1541. [CrossRef] [PubMed]

153. Dalton, a Molecular Electronic Structure Program, Release 2.0 (2005). Available online: http://daltonprogram.org/ (accessed on 29 December 2016).

154. Pierloot, K.; Vancoillie, S. Relative Energy of the High-(^{5}T$_{2g}$) and Low-(^{1}A$_{1g}$) Spin States of [Fe(H$_2$O)$_6$]$^{2+}$, [Fe(NH$_3$)$_6$]$^{2+}$, and [Fe(bpy)$_3$]$^{2+}$: CASPT2 Versus Density Functional Theory. *J. Chem. Phys.* **2006**, *125*, 124303. [CrossRef] [PubMed]

155. Gindensperger, E.; Koppel, H.; Daniel, C. Mechanism of Visible-Light Photoisomerization of a Rhenium(I) Carbonyl-Diimine Complex. *Chem. Comm.* **2010**, *46*, 8225–8227. [CrossRef] [PubMed]

156. Escudero, D.; Thiel, W. Assessing the Density Functional Theory-Based Multireference Configuration Interaction (DFT/MRCI) Method for Transition Metal Complexes. *J. Chem. Phys.* **2014**, *140*, 194105. [CrossRef] [PubMed]

157. Domingo, A.; Carvajal, M.; de Graaf, C.; Sivalingam, K.; Neese, F.; Angeli, C. Metal-to-Metal Charge-Transfer Transitions: Reliable Excitation Energies from Ab Initio Calculations. *Theor. Chem. Acc.* **2012**, *131*, 1–13. [CrossRef]

158. De Angelis, F.; Fantacci, S.; Selloni, A.; Nazeeruddin, M.K.; Graetzel, M. Time-Dependent Density Functional Theory Investigations on the Excited States of Ru(II)-Dye-Sensitized TiO$_2$ Nanoparticles: The Role of Sensitizer Protonation. *J. Am. Chem. Soc.* **2007**, *129*, 14156–14157. [CrossRef] [PubMed]

159. De Angelis, F.; Fantacci, S.; Selloni, A.; Nazeeruddin, M.K.; Grätzel, M. First-Principles Modeling of the Adsorption Geometry and Electronic Structure of Ru(II) Dyes on Extended TiO$_2$ Substrates for Dye-Sensitized Solar Cell Applications. *J. Phys. Chem. C* **2010**, *114*, 6054–6061. [CrossRef]

160. Wiberg, J.; Marinado, T.; Hagberg, D.P.; Sun, L.; Hagfeldt, A.; Albinsson, B. Effect of Anchoring Group on Electron Injection and Recombination Dynamics in Organic Dye-Sensitized Solar Cells. *J. Phys. Chem. C* **2009**, *113*, 3881–3886. [CrossRef]

161. Pastore, M.; De Angelis, F. Aggregation of Organic Dyes on TiO$_2$ in Dye-Sensitized Solar Cells Models: An Ab Initio Investigation. *ACS Nano* **2010**, *4*, 556–562. [CrossRef] [PubMed]

162. Pastore, M.; De Angelis, F. Computational Modelling of TiO$_2$ Surfaces Sensitized by Organic Dyes with Different Anchoring Groups: Adsorption Modes, Electronic Structure and Implication for Electron Injection/Recombination. *Phys. Chem. Chem. Phys.* **2012**, *14*, 920–928. [CrossRef] [PubMed]

163. Grätzel, M. Conversion of Sunlight to Electric Power by Nanocrystalline Dye-Sensitized Solar Cells. *J. Photochem. Photobiol. A* **2004**, *164*, 3–14. [CrossRef]

164. Odobel, F.; Blart, E.; Lagrée, M.; Villieras, M.; Boujtita, H.; El Murr, N.; Caramori, S.; Bignozzi, C.A. Porphyrin Dyes for TiO$_2$ Sensitization. *J. Mater. Chem.* **2003**, *13*, 502–510. [CrossRef]

165. Abbotto, A.; Manfredi, N.; Marinzi, C.; De Angelis, F.; Mosconi, E.; Yum, J.; Xianxi, Z.; Nazeeruddin, M.K.; Grätzel, M. Di-Branched Di-Anchoring Organic Dyes for Dye-Sensitized Solar Cells. *Energy Environ. Sci.* **2009**, *2*, 1094. [CrossRef]

166. Anselmi, C.; Mosconi, E.; Pastore, M.; Ronca, E.; De Angelis, F. Adsorption of Organic Dyes on TiO$_2$ Surfaces in Dye-Sensitized Solar Cells: Interplay of Theory and Experiment. *Phy. Chem. Chem. Phys.* **2012**, *14*, 15963–15974. [CrossRef] [PubMed]

167. Schiffmann, F.; VandeVondele, J.; Hutter, J.; Wirz, R.; Urakawa, A.; Baiker, A. Protonation-Dependent Binding of Ruthenium Bipyridyl Complexes to the Anatase(101) Surface. *J. Phys. Chem. C* **2010**, *114*, 8398–8404. [CrossRef]

168. De Angelis, F.; Vitillaro, G.; Kavan, L.; Nazeeruddin, M.K.; Grätzel, M. Modeling Ruthenium-Dye-Sensitized TiO$_2$ Surfaces Exposing the (001) or (101) Faces: A First-Principles Investigation. *J. Phys. Chem. C* **2012**, *116*, 18124–18131. [CrossRef]

169. Pastore, M.; De Angelis, F. First-Principles Computational Modeling of Fluorescence Resonance Energy Transfer in Co-Sensitized Dye Solar Cells. *J. Phys. Chem. Lett.* **2012**, *3*, 2146–2153. [CrossRef] [PubMed]

170. Ronca, E.; Pastore, M.; Belpassi, L.; Tarantelli, F.; De Angelis, F. Influence of the Dye Molecular Structure on the TiO$_2$ Conduction Band in Dye-Sensitized Solar Cells: Disentangling Charge Transfer and Electrostatic Effects. *Energy Environ. Sci.* **2013**, *6*, 183–193. [CrossRef]

171. Kang, W.; Hybertsen, M.S. Quasiparticle and Optical Properties of Rutile and Anatase TiO$_2$. *Phys. Rev. B* **2010**, *82*, 085203. [CrossRef]

172. Chiodo, L.; Garc√≠a-Lastra, J.M.; Iacomino, A.; Ossicini, S.; Zhao, J.; Petek, H.; Rubio, A. Self-Energy and Excitonic Effects in the Electronic and Optical Properties of TiO$_2$ Crystalline Phases. *Phys. Rev. B* **2010**, *82*, 045207. [CrossRef]

173. Landmann, M.; Rauls, E.; Schmidt, W.G. The Electronic Structure and Optical Response of Rutile, Anatase and Brookite TiO$_2$. *J. Phys. Condens. Matter* **2012**, *24*, 195503. [CrossRef] [PubMed]

174. Park, Y.R.; Kim, K.J. Structural and Optical Properties of Rutile and Anatase TiO$_2$ Thin Films: Effects of Co Doping. *Thin Solid Films* **2005**, *484*, 34–38. [CrossRef]

175. Neaton, J.B.; Hybertsen, M.S.; Louie, S.G. Renormalization of Molecular Electronic Levels at Metal-Molecule Interfaces. *Phys. Rev. Lett.* **2006**, *97*, 216405. [CrossRef] [PubMed]

176. Persson, P.; Lundqvist, M.J.; Ernstorfer, R.; Goddard, W.A.; Willig, F. Quantum Chemical Calculations of the Influence of Anchor-Cum-Spacer Groups on Femtosecond Electron Transfer Times in Dye-Sensitized Semiconductor Nanocrystals. *J. Chem. Theory Comput.* **2006**, *2*, 441–451. [CrossRef] [PubMed]

177. Muscat, J.P.; Newns, D.M. Chemisorption on Metals. *Prog. Surf. Sci.* **1978**, *9*, 1–43. [CrossRef]

178. Lundqvist, M.J.; Nilsing, M.; Persson, P.; Lunel, S. DFT Study of Bare and Dye-Sensitized TiO$_2$ Clusters and Nanocrystals. *Int. J. Quantum Chem.* **2006**, *106*, 3214–3234. [CrossRef]

179. De Angelis, F.; Fantacci, S.; Mosconi, E.; Nazeeruddin, M.K.; Grätzel, M. Absorption Spectra and Excited State Energy Levels of the N719 Dye on TiO$_2$ in Dye-Sensitized Solar Cell Models. *J. Phys. Chem. C* **2011**, *115*, 8825–8831. [CrossRef]

180. Caramori, S.; Ronconi, F.; Argazzi, R.; Carli, S.; Boaretto, R.; Busatto, E.; Bignozzi, C.A. Solar Energy Conversion in Photoelectrochemical Systems. In *Applied Photochemistry: When Light Meets Molecules*; Bergamini, G., Silvi, S., Eds.; Springer: Cham, Switzerland, 2016; pp. 67–143.

181. Youngblood, W.J.; Lee, S.-H.A.; Kobayashi, Y.; Hernandez-Pagan, E.A.; Hoertz, P.G.; Moore, T.A.; Moore, A.L.; Gust, D.; Mallouk, T.E. Photoassisted Overall Water Splitting in a Visible Light-Absorbing Dye-Sensitized Photoelectrochemical Cell. *J. Am. Chem. Soc.* **2009**, *131*, 926–927. [CrossRef] [PubMed]

182. Hoertz, P.G.; Kim, Y.-I.; Youngblood, W.J.; Mallouk, T.E. Bidentate Dicarboxylate Capping Groups and Photosensitizers Control the Size of IrO$_2$ Nanoparticle Catalysts for Water Oxidation. *J. Phys. Chem. B* **2007**, *111*, 6845–6856. [CrossRef] [PubMed]

183. She, C.; Guo, J.; Irle, S.; Morokuma, K.; Mohler, D.L.; Zabri, H.; Odobel, F.; Youm, K.-T.; Liu, F.; Hupp, J.T.; et al. Comparison of Interfacial Electron Transfer through Carboxylate and Phosphonate Anchoring Groups†. *J. Phys. Chem. A* **2007**, *111*, 6832–6842. [CrossRef] [PubMed]